GeoHazards

Tracked for Impact Factor

CITESCORE 2.6

Article

Deep Electrical Resistivity Tomography for Detecting Gravitational Morpho-Structures in the Becca France Area (Aosta Valley, NW Italy)

Maria Gabriella Forno, Marco Gattiglio, Franco Gianotti, Cesare Comina, Andrea Vergnano and Stefano Dolce

Special Issue

Landslide Research: State of the Art and Innovations

Edited by

Dr. Davide Tiranti

MDPI

https://doi.org/10.3390/geohazards5030045

GeoHazards

MDPI

Article

Deep Electrical Resistivity Tomography for Detecting Gravitational Morpho-Structures in the Becca France Area (Aosta Valley, NW Italy)

Maria Gabriella Forno *, Marco Gattiglio, Franco Gianotti, Cesare Comina, Andrea Vergnano and Stefano Dolce

Department of Earth Sciences, University of Turin, Via Valperga Caluso 35, 10125 Turin, Italy; marco.gattiglio@unito.it (M.G.); franco.gianotti@unito.it (F.G.); cesare.comina@unito.it (C.C.); andrea.vergnano@unito.it (A.V.); stefano.dolce996@edu.unito.it (S.D.)

* Correspondence: gabriella.forno@unito.it

Abstract: Deep-seated gravitational slope deformations (DSGSDs) consist of gravity-induced, large-scale, gradual rock mass movements. In the Aosta Valley region (Valle d'Aosta NW Italy), DSGDs affect wide valley slopes and produce several interconnected morpho-structures that involve bedrock and Quaternary cover. Some DSGSD effects are not visible at the surface because of subglacial abrasion or burial by sediments and, therefore, are difficult to map with standard geomorphological surveys. This is the case for the Pointe Leysser DSGSD in the Aosta Valley, which is heavily influenced by the historical movements of the Verrogne-Clusellaz Glacier and its tributaries. We conducted a new geological investigation, integrated with deep electrical resistivity tomography geophysical surveys (ERTs). The ERT results were initially compared with geological/geomorphological evidence at the surface to define the correlation between the values and spatial distributions of electrical resistivity and the sediments, rocks, or morpho-structures. The resistivity values at various depths were subsequently analysed, interpreted, and discussed in conjunction with geological hypotheses. The geological and geophysical survey revealed three wide buried glacial valleys filled with glacial sediments and mapped the locations of gravitational morpho-structures at depth. These new data allowed us to draw a relationship between glacialism and gravitational evolution, distinguishing between pre-singlacial movements and postglacial movements.

Keywords: electrical resistivity tomography (ERT); gravitational morpho-structures; Becca France; Val Clusellaz; Last Glacial Maximum (LGM)-Holocene; deep-seated gravitational slope deformation (DSGSD)

Citation: Forno, M.G.; Gattiglio, M.; Gianotti, F.; Comina, C.; Vergnano, A.; Dolce, S. Deep Electrical Resistivity Tomography for Detecting Gravitational Morpho-Structures in the Becca France Area (Aosta Valley, NW Italy). *GeoHazards* **2024**, *5*, 886–916. https://doi.org/10.3390/geohazards5030045

Academic Editor: Davide Tiranti

Received: 29 June 2024
Revised: 29 August 2024
Accepted: 30 August 2024
Published: 9 September 2024

1. Introduction

Deep-seated gravitational slope deformation (DSGSD) is one of the main modelling factors of uplifting orogenic chains. The gravity-induced evolution can be associated with the last deformation step of the chains. These gravitational deformation phenomena develop very slowly and evolve over long periods [1–11]. Usually, as in NW Italy, DSGSDs have variably fractured bedrock and complex structural settings due to several morpho-structures of various types (mainly doubled ridges, minor scarps, trenches, counterscarps, and tilted bedrock blocks), locations (from watershed to valley floors), extents (up to a few tens km^2), and ages (essentially from Lateglacial to Holocene).

This work improves the understanding of a specific research area within the Aosta Valley, where DSGSD movements and glacial shaping overlap in complex ways. The area, approximately 10 km W of Aosta town, is located in the middle Aosta Valley, near the Becca France ridge within the Pointe Leysser DSGSD on the hydrographic left (Figure 1). The Clusellaz and Clapin torrents, which flow towards the ESE, and the de Morgnoz and de Fourmière minor torrents, which flow towards the SE, drain this sector (Figure 2).

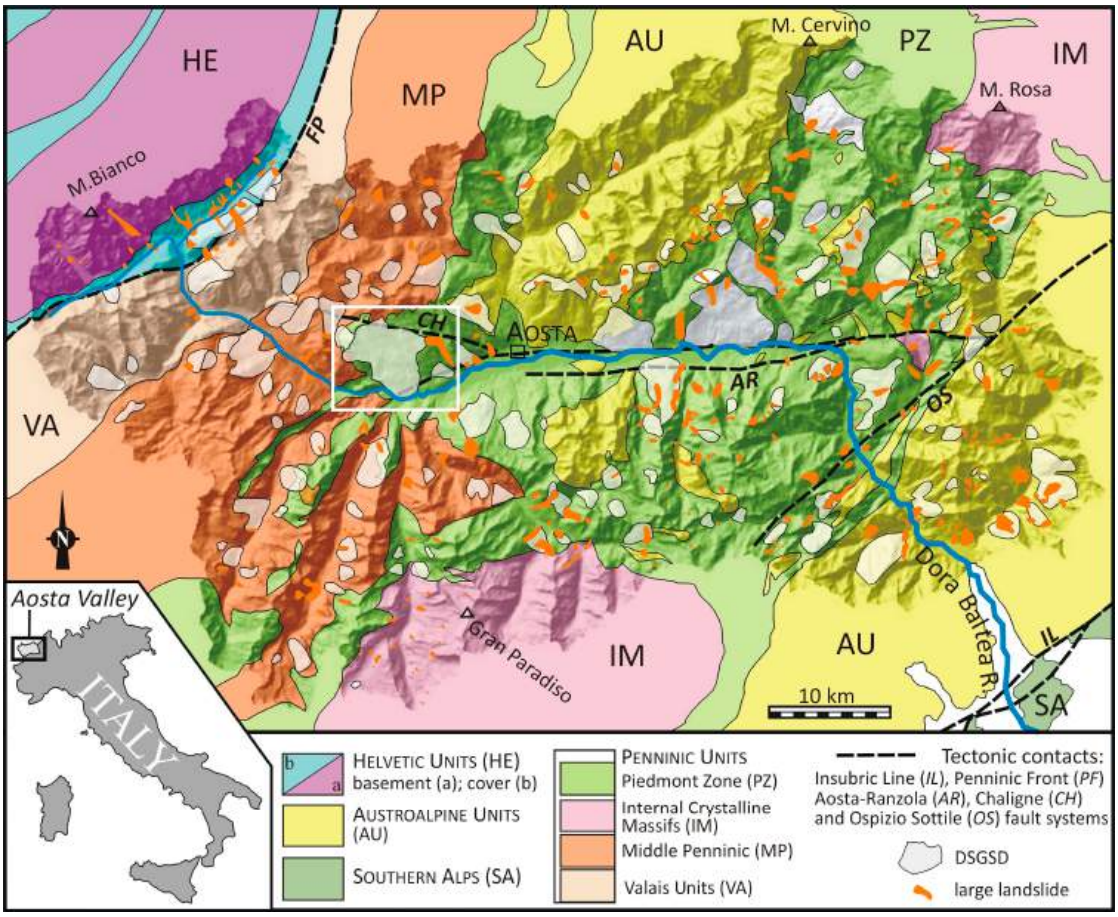

Figure 1. Geological sketch of the Aosta Valley with the location of the Pointe Leysser DSGSD (white square) (from [12]).

Various examples of DSGSD morpho-structures reshaped by glaciers are recognised in this sector, as are the cases of exposed glacial sediments and landforms displaced by gravitational elements [5].

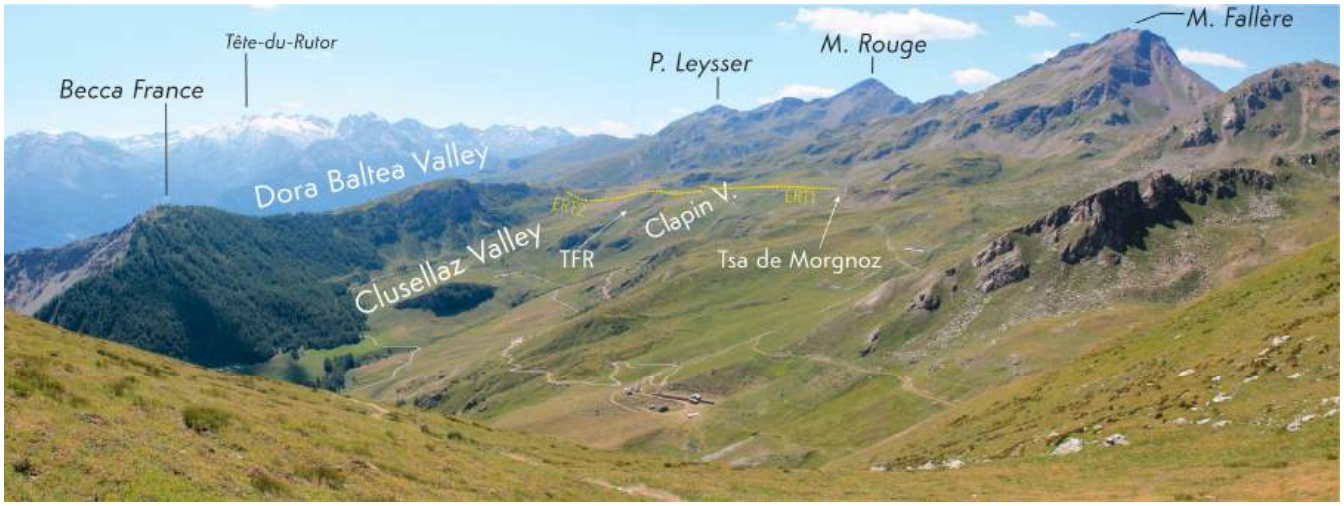

Figure 2. General view of Clusellaz and Clapin Valleys, separated by the Tsa de Fourmière Relief (TFR) and investigated by the ERT1 and ERT2 profiles, and bordered by the ridges of Mont Fallère and Becca France (the distance from Mont Fallère and Becca France is approximately 3500 m).

The interplay between gravitational movements and glacial shaping implies that not all gravitational morpho-structures are well exposed and easy to recognise since several of them have been reshaped by subglacial abrasion or are buried under glacial and other types of sediments. Outcropping gravitational structures can be efficiently mapped through direct observations by field geologists and specific geological surveys. In contrast, buried gravitational structures can be recognised only by underground investigations, i.e., geophysical surveys. Among the available geophysical methods, electric resistivity tomography (ERT) is commonly used to image near-surface conditions and diagnose slope instabilities. Several deformation structures can be identified by surveying the electrical resistivity of bedrock and sediments underlying a defined profile line, e.g., [13–16]. The application of ERT in DSGSD environments has already been reported in several examples in the literature, e.g., [17–20] providing valuable underground information to complement surficial geological evidence. The limited access to the terrain and the mountain-scale extension of DSGSDs, which often encompass entire valley flanks and various thicknesses, might make it difficult to use ERT to investigate the depths of these failures. As a result, few studies have documented the use of ERT to analyse the geological and structural conditions of bedrock at relatively great depths.

This work is, therefore, focused on the combination of detailed ERT surveys and specific geological investigations for the detection of all the gravity-induced structures of the investigated sector at a large scale to connect the outcropping elements with the buried elements and completely reconstruct the geological setting of the area related to both DSGSD and glacial shaping. This work will also provide an operational framework for DSGSD and glacial landform studies in mountain areas where the application of combined geological and geophysical methodologies is still lacking.

2. Features of Deep-Seated Gravitational Slope Deformation

DSGSDs are large-scale rock mass movements with very low velocities (few mm/year) which comprise entire valley flanks and involve both bedrock and Quaternary cover [21–32].

The DSGSDs involve slopes with high relief energy, foliated rocks, highly fractured rocks connected with brittle tectonic deformation and locally deep dissolution of sulphate and carbonate rocks [33–38]. Changes in the volumes of glaciers over time have also closely conditioned the evolution of Alpine DSGSDs, and particularly the postglacial debuttressing promoted these gravitational phenomena [39,40].

These gravitational phenomena increase the fracturing of the rock mass and trigger a widespread opening of new and preexisting fractures, with volumes characterised by a substantial incoherence in the bedrock which appears wholly loosened. The slope involved in a DSGSD exhibits fractures, which are decimetric to decametric in length, have centimetric to metric opening and promote differential slope instabilities (persistent joints in [41]). Consequently, the slope shows a complex morpho-structural setting, resulting in a typical gravitational morphology, often characterised by a step-like profile and a cone shape in the more active sector [42–44]. The DSGSD produce different types of landforms (morpho-structures) of various sizes, such as doubled ridges, minor scarps, trenches, counterscarps, and bulging reliefs which testify to the slow deformation of the long-lasting DSGSD [23,45].

Doubled ridges are elongated depressions along the watershed resulting in the extension of mountain ridges, with doubled or multiple rocky reliefs which are often the most evident and extensive morpho-structures of gravitational deformation (several hundred metres in length and several tens of metres in depth).

Trenches typically consist of elongated depressions along DSGSD slopes, whose dimensions vary from a few metres to hundreds of metres in length and up to tens of metres in depth. Trenches are formed by the further widening of open fractures, involving volumes of bedrock with Quaternary cover. Trenches can align in the same direction as altitude contour lines (transversal trenches) or according to the maximum slope (longitudinal trenches) [46].

Minor scarps consist of facing-downstream walls in DSGSDs where bedrock and Quaternary cover are affected by gravitational slip, creating a typical set of varying-size

steps. In contrast, counterscarps are face-upstream walls where the slope slides in the opposite direction compared with the scarps [47].

Tilted bedrock blocks consist of wide slabs gravitationally displaced on listric sliding surfaces [48].

Bulging reliefs, recognised in some DSGSDs, consist of isolated rocky reliefs in a perched position rather than in the surrounding areas [43,46–49]. Rocky volumes form these reliefs, bounded upstream by a trench (wherein subglacial sediments are abundant) and downstream by a subvertical rocky scarp which results in a prominent frontal edge. These structures often open and slide along straight or concave surfaces, dislocating bedrock and sediments.

In addition, asymmetrical valleys are detected in several DSGSDs with very different elevations between two flanks, with higher slopes formed by fewer fractured rocks than the other slopes. These peculiar valleys, defined as gravitational valleys [46], are consequent to the opening and gravitational sliding of a slope, with a minor elevation of the slipped mountainside, and have a different origin than traditional glacial or fluvial valleys. Alpine gravitational valleys are due to the evolution of gravitational sliding surfaces over very long timescales, which are subsequently deepened by watercourses or glaciers.

Unlike most regional tectonic structures, which essentially affect bedrock, DSGSD phenomena also involve Quaternary sediments and landforms. In addition, the Quaternary succession connected to DSGSDs shows typical facies characterised by the abundance of small (centimetre-sized) angular and monogenic clasts with a scarce matrix [30].

DSGSDs are common on all mountain chains and are especially large and numerous in the Alps, essentially in deep valleys shaped by glaciers during glaciations and the subsequent river erosion [1,24–32]. DSGSDs are also frequent in the western Alpine Chain and involve widespread areas and significant rocky masses [50]. Several DSGSDs are mapped in the IFFI Inventory (Inventario Fenomeni Franosi Italia) of the Dora Baltea Valley (Aosta Valley), where these phenomena cover an area of 460 km^2, resulting in approximately 25% of all the recognised DSGSDs in the Italian Alps [51,52]. The DSGSDs of the Western Alps, which are particularly common between 1000 and 1700 m a.s.l., show significant variability in spatial extent, deformation mechanisms, and the state of activity [35]. These gravitational phenomena involve mainly anisotropic rocks, such as calcschist, micaschist, paragneiss, and serpentine-schist, related to the different continental and oceanic tectonometamorphic units of the Alpine axial zone (Figure 1) [43]. The DSGSDs are mainly extensive in the middle sector of the Dora Baltea Valley, with a mean slope gradient varying between 20° and 35° [35]. The tributary lateral valleys, where the topographic elevation is on average higher and the slope gradient is greater, varying between 30° and 35°, conversely exhibit few gravitational phenomena [42].

The DSGSDs located in the Aosta Valley developed in a sector of the Alpine Chain that experienced different significant episodes of glacial expansion, as indicated by the wide distribution of glacial sediments and landforms (Figure 1). In addition, evidence of the last glacial expansion (Last Glacial Maximum, namely global-LGM, 27.5–23.7 ka cal BP according to [53]; or local alpine-LGM, 26.5–19 ka BP according to [54]) and the subsequent postglacial debuttressing appear to involve numerous gravitational movements affecting glacially shaped valley slopes. Consequently, gravitational movements and glacialism, the main phenomena responsible for the recent geological evolution in the Aosta Valley, interact with each other [30,55].

3. Geomorphological and Geological Setting

The Pointe Leysser DSGSD (Figure 3), with an extension of more than 30 km^2, is located in the middle Aosta Valley, a 92 km-long alpine valley shaped during the Pleistocene by the vast Dora Baltea Glacier and its tributaries (Figure 2). This area extends on the southern-facing side of this valley, downstream of the Pointe Leysser (2770 m a.s.l.), Mont Fallère (3061 m), and M. Aouilletta (2616 m) rocky ridge, ranging at altitudes from 2200 to 2250 m, approximately 10 km W of Aosta town [50,56–58].

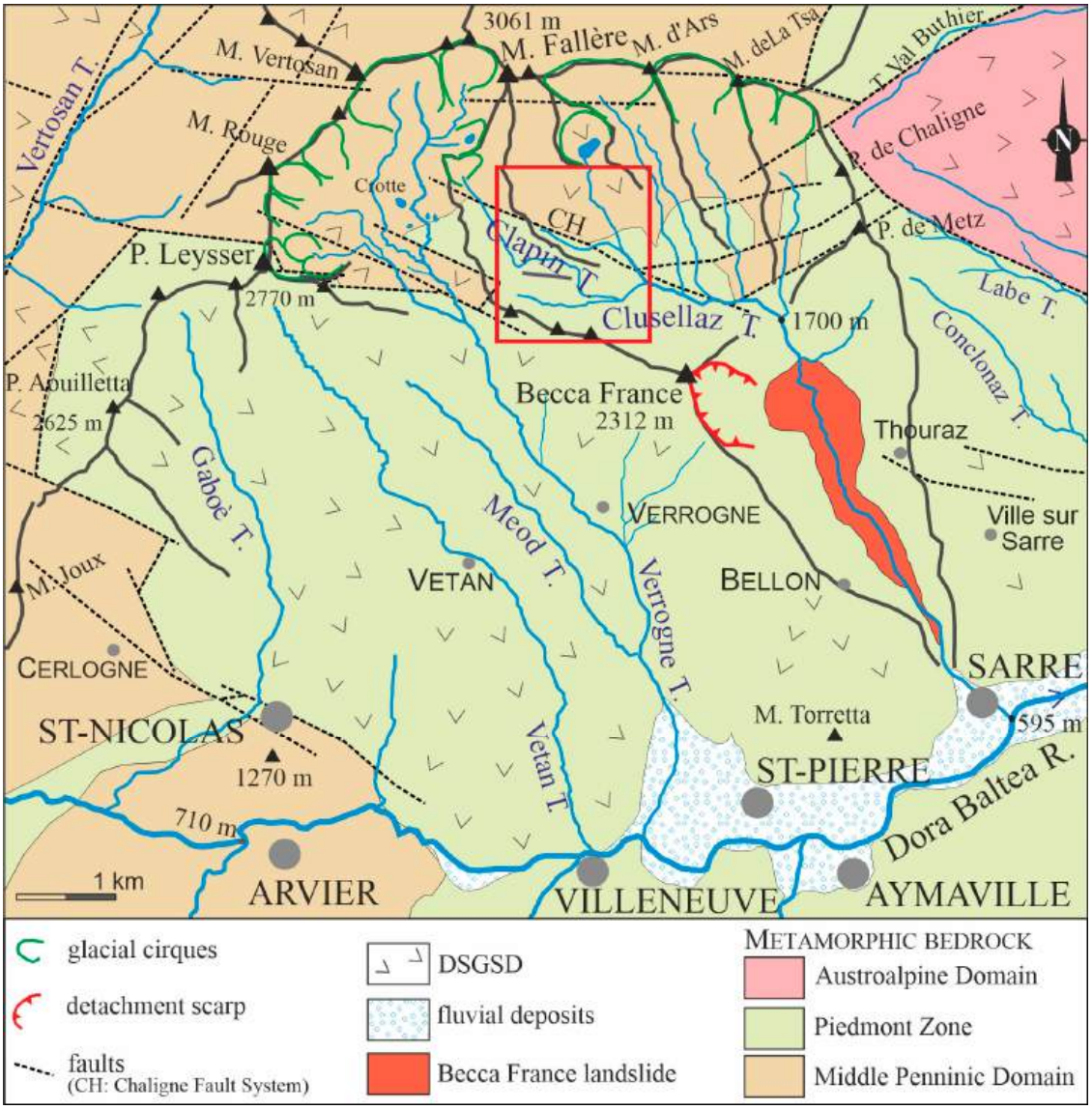

Figure 3. Simplified geological map of the Pointe Leysser DSGSD (white box in Figure 1) modified from [3] (for the tectonic sketch) and from [5] (for the Fallère Lake area). The red rectangle indicates the investigated area.

This sector of the slope, bounded by T. Gaboè and T. Clusellaz (tributaries of the Dora Baltea R.), shows articulated morphology due to the presence of rocky ridges separated by elongated depressions. The prominent WNW–ESE rocky ridge (Becca France) rises above the Clusellaz Valley floor by approximately 300–400 m. Significant doubled ridges characterise it. The main depression consists of a wide valley (Clusellaz Valley continuing upstream with Plan di Modzon) which separates the Becca France ridge from the Tsa de Fourmière Relief (Figure 4).

The Pointe Leysser DSGSD is located along the boundary between the continental Gran San Bernardo Nappe (Middle Penninic Domain) and the above-oceanic Piedmont Zone [59]. This boundary presents several faults related to the NW–SE Chaligne Fault System [3] (Figure 3). Other NE–SW faults correspond to the Gignod System [56,60].

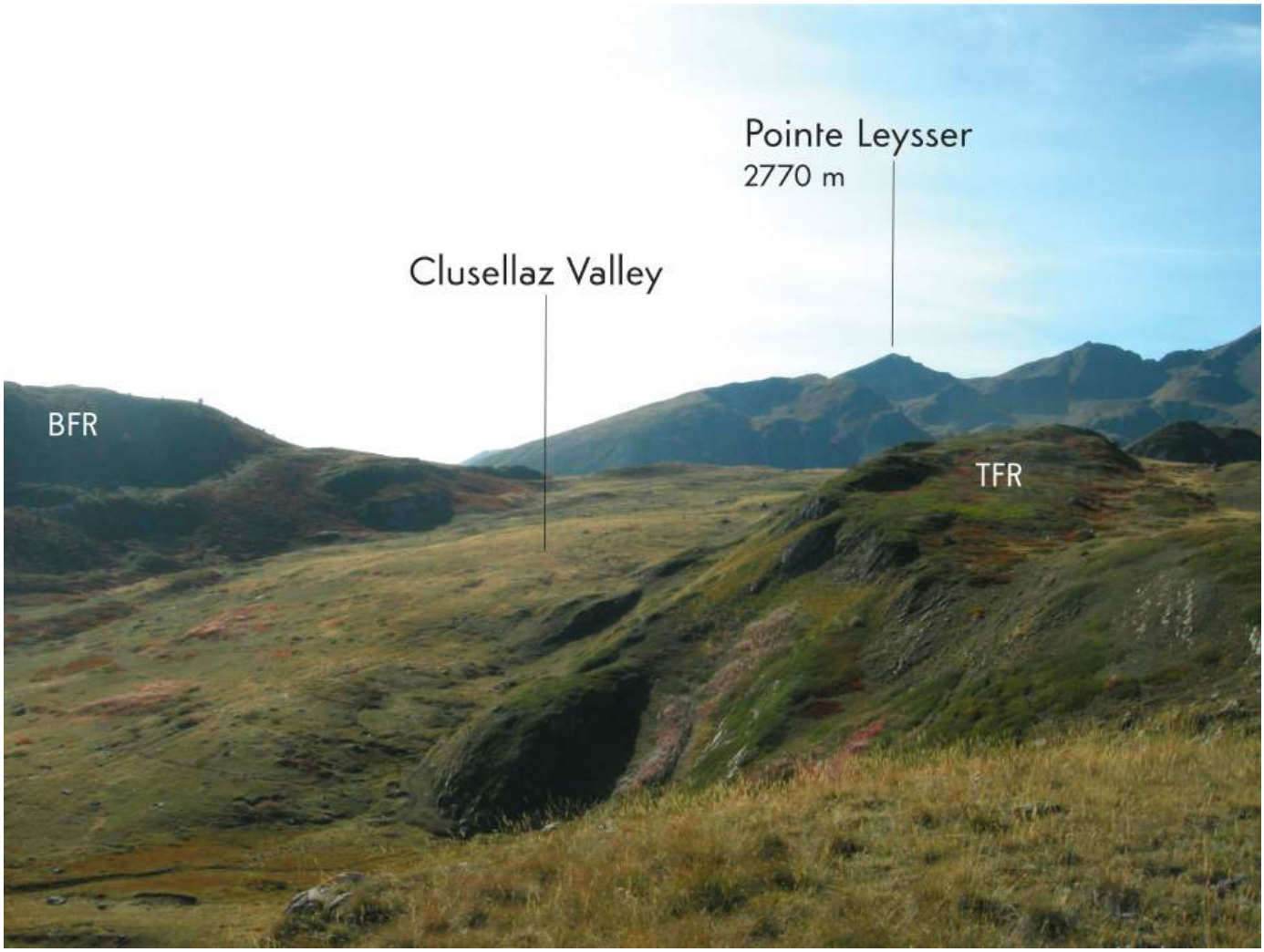

Figure 4. Wide asymmetrical Clusellaz Valley between the Becca France ridge (BFR) and the Tsa de Fourmière Relief (TFR) (the distance between BFR and TFR shown in the figure is approximately 470 m).

The bedrock in the area is shaped by glaciers and discontinuously hidden by the glacial sediments (consisting of subglacial, ice-marginal, and supraglacial sediments) of the Verrogne-Clusellaz Glacier and its tributaries, which flowed during the LGM and Lateglacial. Additionally, more localised torrential, landslide, debris, and palustrine sediments locally cover the bedrock and glacial sediments.

The Pointe Leysser DSGSD area features large rocky volumes of very fractured and loose rocks, characterised by several systems of open fractures. Consequently, many outcrops of "in situ" rocks are formed by juxtaposed centimetric angular fragments, which can be confused with Quaternary sediments [30].

The same DSGSD also exhibits several evident outcropping morpho-structures. A complex doubled ridge (often resulting in several coupled depressions up to 20 m deep and 50 m wide) involves the Pointe Leysser–Becca France ridge, with an overall length of up to 2.5 km [61].

Minor scarps are the most widespread gravitational morpho-structures and are very common in the southern slope of the Becca France ridge, in Plan di Modzon, and around the Lac Fallère [12,61,62]. These structures produce curved scarps, plunging downstream and high up to several tens of metres, often oriented according to altitude contour lines. Counterscarps (metric in size and plunging upstream) are located mainly on the northern

slope of the Becca France ridge. Geophysical surveys have also detected several buried counterscarps in Plan di Modzon [17].

Trenches, resulting in elongated depressions (open up to a few metres) oriented mainly along the lines of maximum slope, are common in the southern slope of the Becca France ridge and around the Lac Fallère. Watercourses often flow along trenches, causing their further deepening. Several gravitational depressions contribute to the formation of a complex hydrographic network and various filled lakes, favouring prehistoric human use as high mountain sites [63].

Bulging reliefs of different sizes are situated south of Lac Fallère. The most significant and extensive area barred the glacier once it was hosted in the Fallère glacial cirque [5].

The head of the Clusellaz Valley is in almost continuity with the high Verrogne Valley because of a diversion phenomenon. The Verrogne Glacier, which previously, during the LGM, flowed towards the SE through the Clusellaz Valley, changed its course during the Lateglacial, subsequently flowing in a N–S direction and shaping the low Verrogne Valley. This phenomenon is due to the erosion of rocks weakened by DSGSD fracturing on the originally continuous Becca France ridge (Figure 3) [61].

The Aosta Valley has a temperate oceanic climate that is transitional to hemi-continental and lacks a dry season [64] according to the Strahler climate classification. The climate is extremely variable according to the Köppen classification because of the wide elevation range from the picks and valley floors and consequently, the complex orography of this region [65]. The climate is classified as alpine frost (EF) or alpine tundra (ET) at relatively high elevations (above 2000 m a.s.l.) owing to an average temperature below 10 °C. In contrast, a boreal climate with warm summers characterises valley slopes and a warm temperate climate is typical of tributary valley bottoms. Moreover, the middle Dora Baltea Valley floor has an arid–semiarid climate, resulting in one of the driest sites in the Alps (550 mm/y of precipitation in the S. Marcel locality).

The mean annual temperature is 10–12 °C in the valley floor and 7.5 °C at 1200 m.

Rainstorms are common in July and, to a lesser degree, in August. The region has an alpine sublittoral pluviometric regime, with two maxima in the middle seasons and two minima in the summer and winter. The average annual precipitation is 658 mm (with a maximum of 75.1 mm in October and a minimum of 40 mm in February) at the Saint Nicolas weather station (dataset 1913–1961). The data calculated for the Crotte Basse site (2365 m a.s.l., close to the Clusellaz Valley head) indicate a mean temperature and precipitation of −6.9 °C and 131 mm in January and 8.6 °C and 97 mm in July, i.e., the coldest and warmest months, respectively (reference period 1961–1990) [66,67].

4. Methods

A detailed geological survey of the bedrock and Quaternary sediments and landforms of the investigated area (at 1:10,000 scale) was integrated with a digital terrain model (2 m DTM 2005–2008 of the Regione Autonoma Valle d'Aosta), producing a new original geological map.

This geological map was created via the ArcGIS Pro software and the "Carta Tecnica Regionale Vettoriale" map at a 1:10,000 scale of the Regione Autonoma Valle d'Aosta 2005–2008 Edition was used as a base. It includes all the topographic elements, such as contour lines, hydrographs, place names, buildings, and roads.

We acquired two ERT lines along two different lineaments, approximately NE–SW (ERT1, length of 960 m) and N–S (ERT2, length of 710 m). The two-day survey took place in September 2023 after a long period of dry conditions. For this reason, each electrode was watered and appropriately coupled to the ground to reduce contact resistance. Data were acquired with a Syscal-Pro georesistivimeter (Iris Instruments) using a set of 48 electrodes at 10 m spacing. To cover the length of the investigated profiles, a 24-electrode superposition was adopted ("roll-along"), and the entire acquisition sequence was repeated for each new survey location. For this reason, ERT1 was performed with three consecutive acquisitions for a total of 96 measuring electrodes, whereas ERT2 was performed via two consecutive

acquisitions for 72 measuring electrodes. The position and elevation of each electrode were obtained via a GNSS EMLID receiver with RTK corrections by the regional satellite positioning system (SPIN 3 GNSS).

We adopted an acquisition sequence based on dipole–dipole quadrupoles for the surveys, with 497 potential readings for every 48-electrode acquisition. The dipole–dipole configuration is appropriate for detecting lateral variations along the profiles as in the aims of the executed surveys. The measurements were repeated on the same quadrupole with the current and voltage electrodes inverted (i.e., reciprocal data) to evaluate data error. The current was injected into the electrodes for 250 ms (milliseconds), with an average injected current of 100 mA (milliampere). A resistivity check was also performed before each acquisition to ensure the goodness of the coupling between the electrodes and the ground (i.e., contact resistance check). Most contact resistances were approximately 5 kilo ohm, with some slightly exceeding 10 kilo ohm. Each measurement was repeated at least 3 times, up to a maximum of 6, and the results were stacked, with an accepted error percentage of 5%.

We postprocessed the acquired data via the ProsysIII software (IRIS instruments), which is able to filter raw ERT data to eliminate outliers (very high or very low resistivity or isolated values) or data with a too-high error percentage. After this preliminary filtering, we imported the data into the ResIPy software (version: 3.5.4) [68] for inversion. A power-law error model was generated on the basis of repeated reciprocal measurements. This error model, a function of resistivity, was used in the inversion to allow the measured data to vary within the error range, thereby enhancing the fit between the measured and calculated models. The data were inverted in 2D, accounting for the topography of the electrodes. We built the mesh for the inversions in ResIPy, with a characteristic length of 1 m near the electrodes, and the cell size varied with depth, with a growth factor of 4. Log-data-based, regularised inversions with linear filtering were performed to obtain the desired RMS of 1, as defined in [69] and in the software user manual (available at http://www.es.lancs.ac.uk/people/amb/Freeware/R2/R2.htm, accessed on 24 July 2024). The process converged in 3 iterations for both ERT profiles.

We interpreted the resistivity sections resulting from the inversions in combination with the evidence from the new geological field survey. We evaluated the correspondence between the outcropping rocks or sediments and the specific resistivity values. This correspondence was also applied to identify the buried geological constitution of different sectors, allowing the integration of the surficial map derived by the geological survey with the subsurface information provided by the geophysical survey.

5. Results

5.1. Results of the Geological Survey

We selected the area between the Clapin and Clusellaz Valleys for its location at the boundary between the Becca France ridge and the southern slope of Mont Fallère (Figure 5). It represents a key area for evaluating the extension and typologies of gravitational morpho-structures in order to understand whether the genesis of these valleys is partly connected to gravity-induced movements.

A new, detailed geological survey was conducted to map the different bedrock rock types, Quaternary sediments, landforms, and tectonic and gravitational structures which allowed the creation of an original geological map (Figure 5).

The study area, which consists of Alpine metamorphic rocks, is located along the highly deformed tectonic contact between the Mont Fort Unit (Distulberg and Mètailler Formations) and the overlying Aouilletta Unit, referred to as the Gran San Bernardo nappe system and Combin Zone, respectively [56,60,70–76].

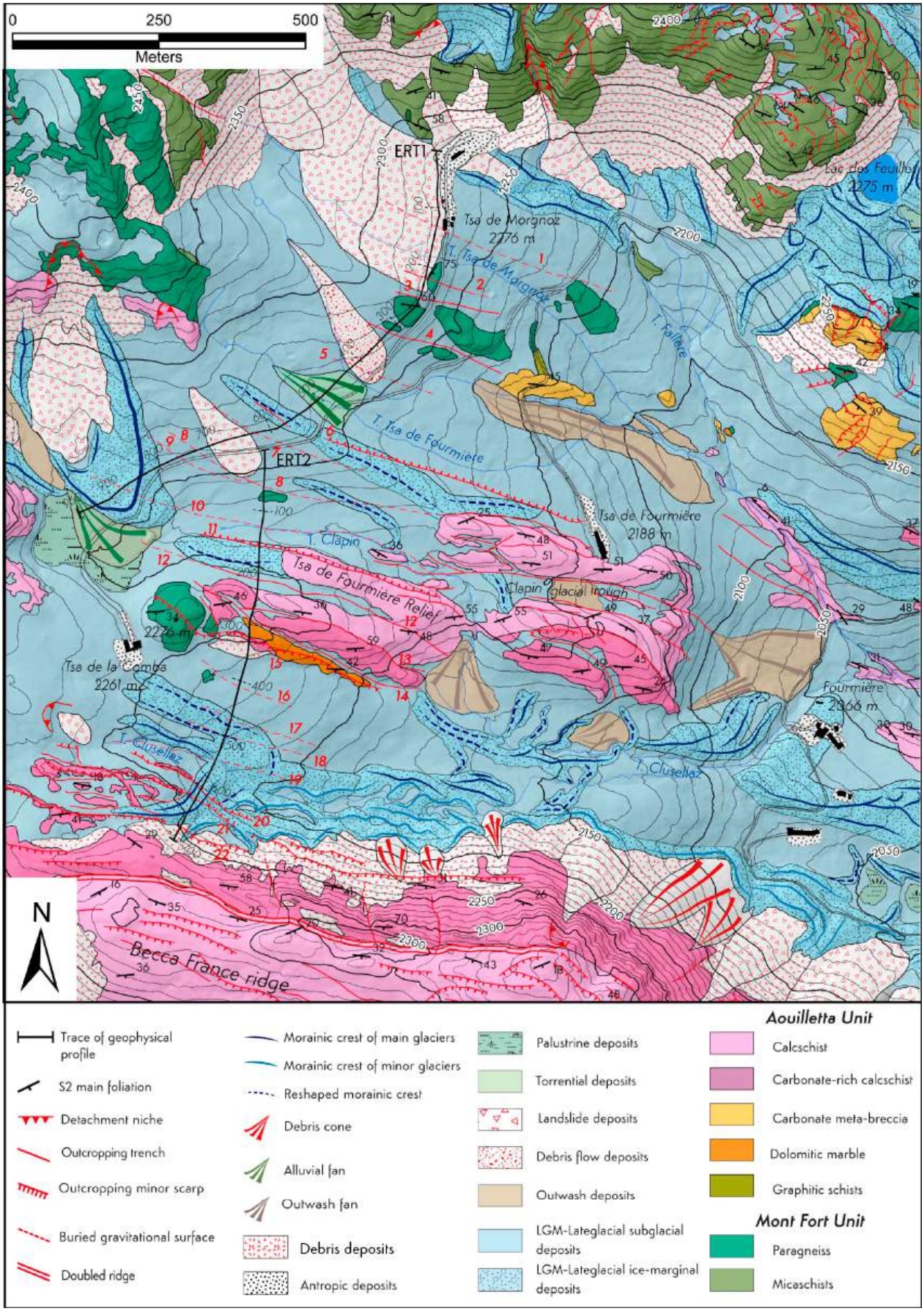

Figure 5. Original geological map of the high Clusellaz Valley, north of the Becca France ridge.

The Distulberg Formation consists mainly of micaschist and paragneiss. The Mètailler Formation consists of various types of gneiss. Metabasic rocks are also present locally in both formations. The Aouilletta Unit also includes, in addition to calcschist, grey and dolomite marble and carbonate meta-breccia with dolomitic pebbles. Four deformation phases are recognisable in the bedrock, the second of which is responsible for the main pervasive foliation (S2). The bedrock does not appear to be homogeneously fractured in the different sectors of the study area, with the depressions essentially developed according to the more fractured rocks and the rocky ridges set in the less fractured rocks.

The morphological findings highlight that the longitudinal trend in the Clapin and upper Clusellaz Valleys, subparallel to the Dora Baltea watershed, represents an atypical feature, which is different from the typical tributary valleys which usually show a path perpendicular to the central valley (Figure 2). Additionally, they clearly show asymmetric profiles. The Clapin Valley has a high left slope with high peaks (Mont Fallère and other picks with altitudes of approximately 3000 m) and several abandoned glacial cirques, and a right low slope which shows, in contrast, a lower altitude (Tsa de Fourmière Relief of some tens of metres). The upper Clusellaz Valley also has a relatively low left slope (Tsa de Fourmière Relief, TFR) and a relatively high right slope (Becca France, with an altitude of 2312 m).

The significantly longer left side exhibits several minor scarps (several metres high) and bulging reliefs (several tens of metres high), resulting in a very articulated morphology that favours the formation of lakes. In contrast, the shorter right side has a series of scarps and counterscarps (several metres high), evidenced by rocky ledges. The presence of several morpho-structures indicates that the origin of the upper Clusellaz Valley is linked to DSGSD movements that typically develop gravitational valleys, as in the other areas where similar landforms are recognised [46].

Remarkably, several hectometric NW–SE rocky ridges separate the wide Clusellaz Valley from the Clapin Valley. Those ridges are part of the Tsa de Fourmière Relief (TFR) (some tens of metres high) (Figure 2). These ridges (parallel to the Becca France ridge and upper Clusellaz Valley floor) are composite because they are formed by several metric to decametric minor ridges and depressions.

The ridges are rounded and show *roches moutonnées* because they experienced glacial shaping. They are cut by rough minor scarps (several metres high) sometimes located along lithological boundaries and by rough close troughs (several metres deep), not involved by glacial shaping, which can be referred to as trenches.

The several depressions in the area result in glacial abandoned valleys that are partly covered by glacial sediments. The extensive glacial cover [47] prevents the detection of possible buried gravitational landforms which only geophysical surveys can identify.

Several moraines (several hundreds of metres long) are observed in the upper Clusellaz Valley, which are arranged according to the valley floor and linked to the main Verrogne-Clusellaz Glacier (Figure 6). In contrast, shorter moraines are observed on its lower right side and are connected to smaller tributary glaciers.

Local debris; torrential sediments, forming small alluvial fans; and landslide sediments are also present.

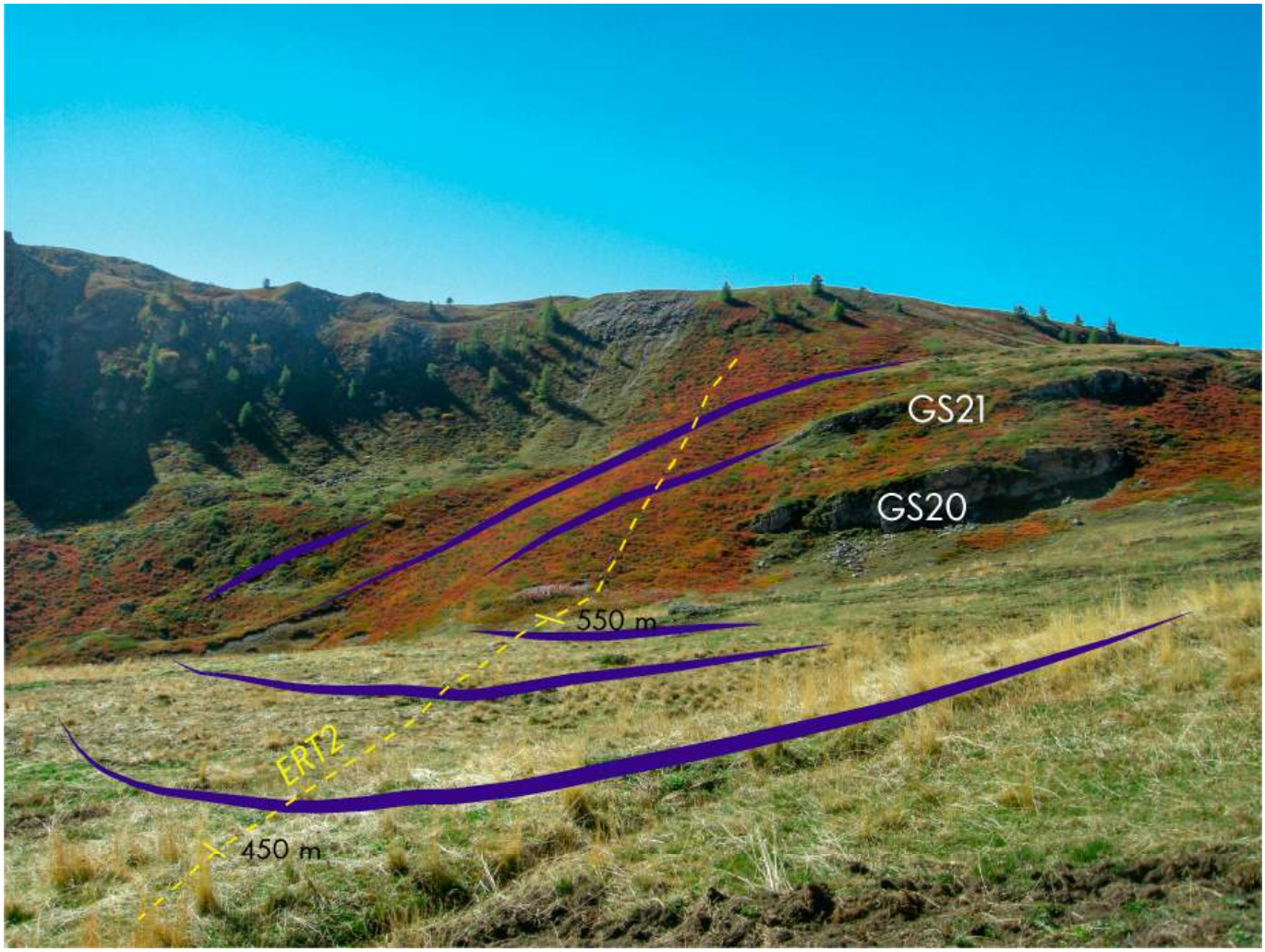

Figure 6. Frontal moraines (light blue lines) in the upper Clusellaz Valley along the ERT2 profile (with a range of 450–550 m), which partly cover the gravitational structures GS**20** and GS**21**.

5.2. Results of Geophysical Investigations

Profile ERT1, with an average elevation of approximately 2280 m and traced perpendicularly to the tributaries of the Fallère Valley, was essentially devoted to investigating the geological framework of the southern Fallère slope in a sector with extensive Quaternary cover (Figure 7). Profile ERT2, with a trace approximately along the direction of the maximum slope of the southern side of M. Fallère, has been used mainly to investigate the geological setting between the T. Fallère slope and the Becca France northern slope, comprising the Clapin Valley and head of Clusellaz Valley, both characterised by a WNW–ESE trend (Figure 7).

The inversion algorithm processed the ERT data to produce the resistivity models of the subsoil, which were interpreted together with geological cross sections (Figure 8A,B).

Along the investigated profiles, the bedrock crops out in the Tsa de Fourmière Relief (TFR) of ERT2 and its terminal portion, i.e., the northern side of the Becca France ridge. It consists of a lithostratigraphic succession of the Aouilletta Unit formed by dolomitic marble, carbonate-rich calcschist and calcschist. The gneiss of the Mont Fort Unit instead more discontinuously outcrops on the northeastern sector of profile ERT1, on the northern side of the Clapin Valley, and at the head of the Clusellaz Valley in ERT2 (Figure 3).

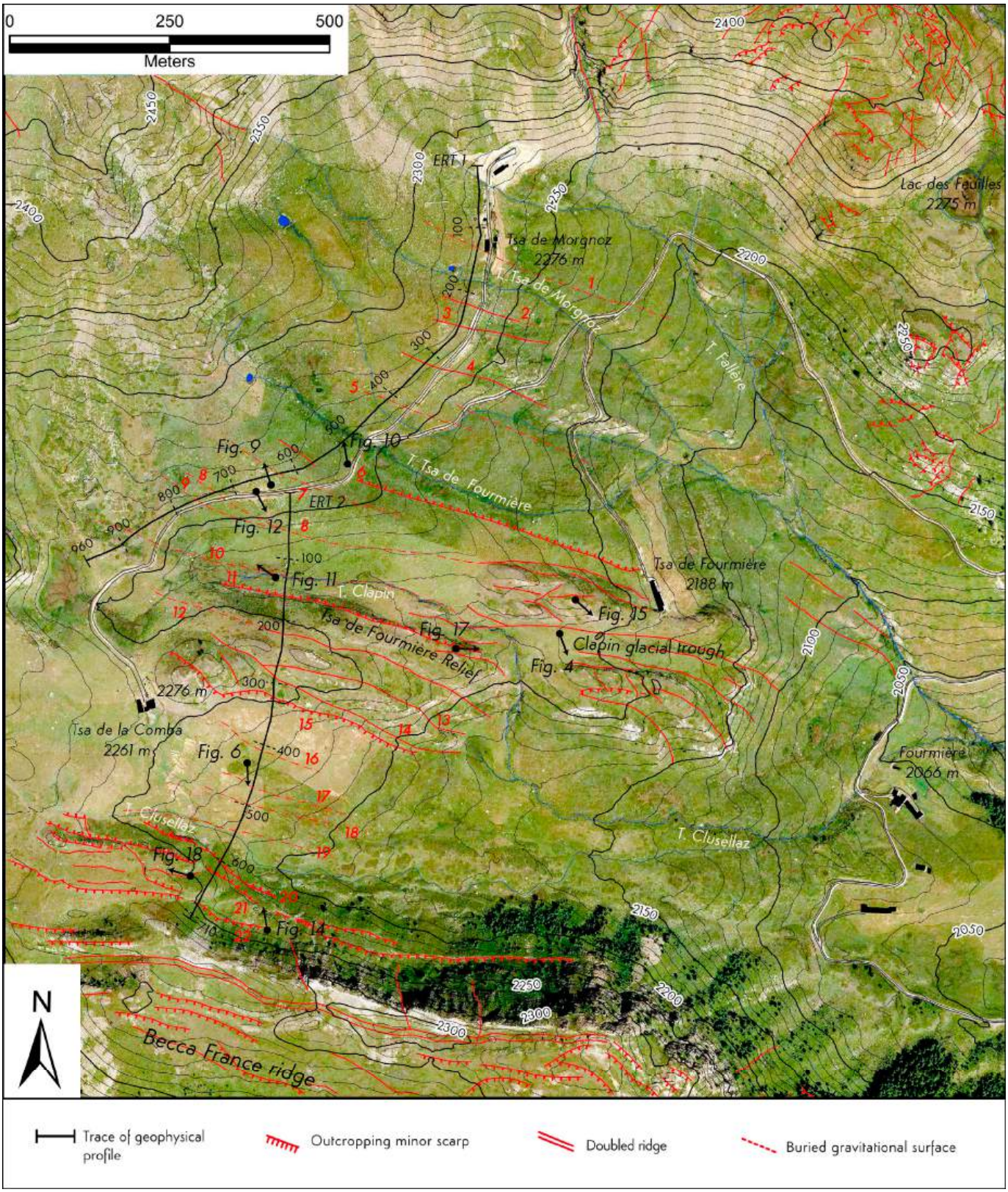

Figure 7. The geoelectric profiles in the high Clusellaz Valley on a Google Earth image with the location of the photographs.

Widespread Quaternary cover was present along the profiles, formed by various sediments with very different features. Subglacial sediments extensively covering the glacial valley floors are highly consolidated and consist of centimetric subangular to

subrounded clasts mixed in a silty–sandy matrix. Ice-marginal sediments, which constitute lateral and frontal moraines in different glacial valleys, are formed by decimetric subangular clasts in a very scarce matrix. More local torrential sediments, which form alluvial fans to different extents, consist of subrounded decimetric to metric clasts mixed in an abundant silty–sandy matrix. Landslide sediments, which form small rockfall accumulations, are composed of variously sized clasts mixed with a scarce matrix.

The bedrock widely shows rounded surfaces linked to subglacial abrasion. In contrast, the local occurrence of rough walls is consistent with gravitational WNW–ESE morpho-structures consisting of scarps dipping towards the south and north. Moreover, WNW–ESE elongated depressions, which often host a subglacial cover, can be related to previous trenches reused by glaciers.

Comparing the surficial geological data with the results of shallow subsoil geophysical investigations makes a more detailed and reliable reconstruction of the geological setting possible. The rocks and sediments outcropping along the profiles, as observed via the geological survey, have potentially different features, resulting in different resistivity values near the surface. Therefore, we used the resistivity values of the outcropping rocks and sediments to define the occurrence of the corresponding buried rocks and sediments. The information deduced from the geophysical profiles is quite reliable for shallow subsoil. However, its validity likely decreases with depth; consequently, the correlation between the resistivity values and rock types becomes less constrained with depth.

Subglacial sediments, which contain an abundant fine matrix that favours water retention, are particularly easy to highlight in geophysical profiles corresponding to a surficial or buried level with low resistivity values. In contrast, dry deposits, due to their high permeability, consisting of prevalent clasts such as ice-marginal, landslide, and torrential sediments, which often lie above subglacial sediments, are emphasised in geophysical profiles by surficial thin high resistivity levels. A slight decrease in the resistivity of these surficial levels may be related to the relatively high water content in the depressions. Poorly fractured bedrock characterised by low permeability is evidenced in geophysical profiles by high resistivity values typical of dry rocks. In contrast, the very fractured and loose bedrock, which has high permeability, is characterised by medium to low resistivity values, suggesting wet rocks.

We describe the geophysical profiles by subdividing them into different stretches, each characterised by homogeneous morphological features and a similar geological setting of the shallow subsoil. The view of the two profiles is from the NW, and the distances are numbered starting from the start of the profiles along the topographic surface. The stretches are indicated by progressive letters in each profile (a, b. . ..), while the structures are enumerated in a continuous progression along the two profiles.

The surficial low to medium resistivity of the first stretch **a** of ERT1 (Figure 8A) (with a range of 0–250 m and a log10 resistivity between 3.2 and 4.0 ohm-metres) suggests a dry rich-in-clast cover. This cover is in agreement with the landslide sediments reported in the geological map that form a wide landslide body supplied by a tributary of the Fallère Basin (Figure 9). The thickness of landslide sediments can differ along the profile (from 15 m in the central stretch to a few metres at both ends).

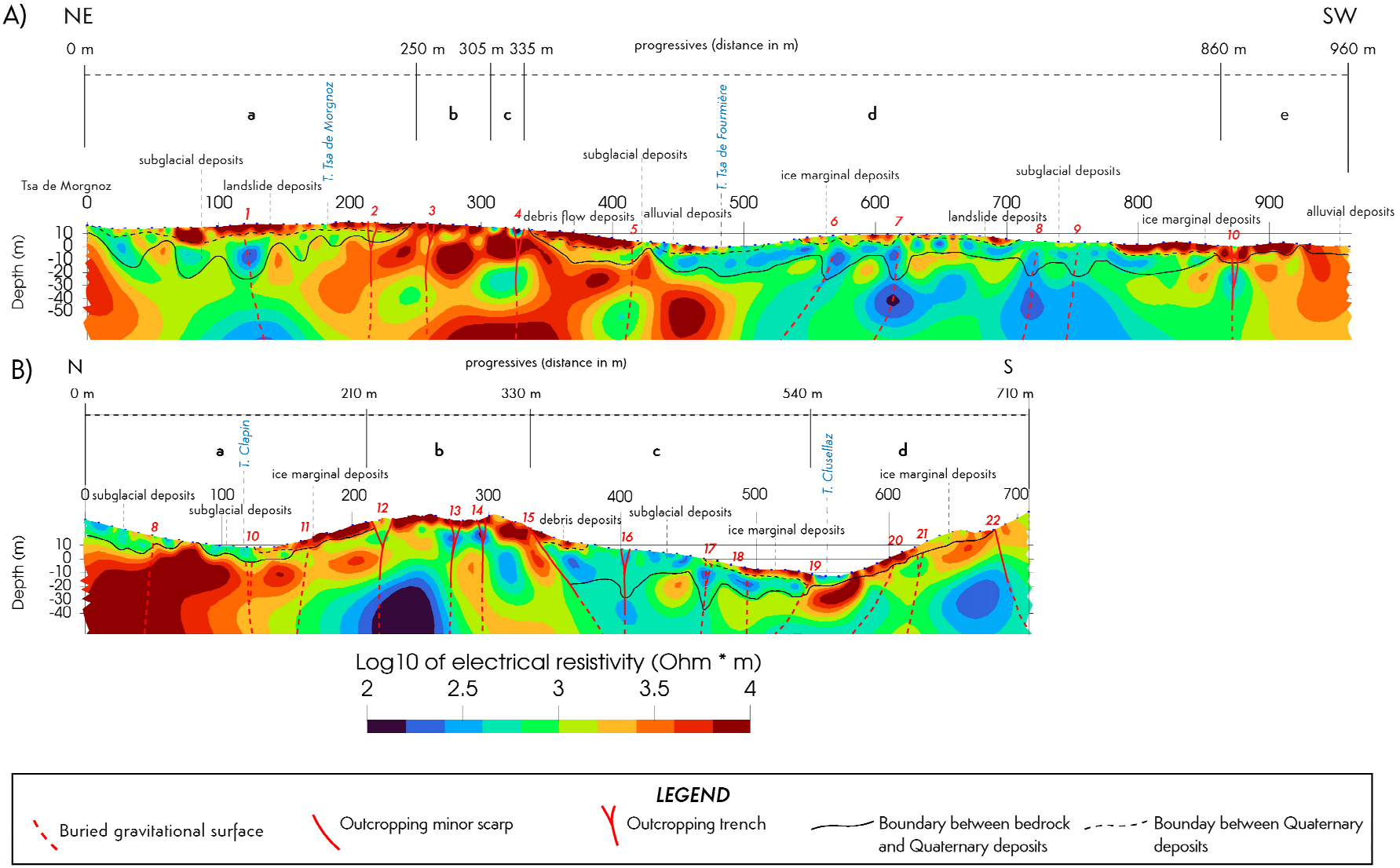

Figure 8. ERT1- (**A**) and ERT2- (**B**) interpreted geophysical profiles seen from NW.

Figure 9. Clast-rich sediments along the stretch **a** of ERT1 (with a range of 600–640 m) form a landslide body (lb) covering the subglacial sediments (in the foreground) (s).

The medium surficial resistivity locally evidenced in this stretch (with a range of 5–15 and 175–185 m and a log10 resistivity between 2.8 and 3.2 ohm-metres) refers to wet sediments along the T. Fallère and T. Tsa de Morgnoz. The low resistivity of the shallow subsoil (with a range of 0–240 m and a log10 resistivity between 2.2 and 3.4 ohm-metres) indicates that thick subglacial sediments (up to approximately 35 m) filled the Tsa de Morgnoz buried glacial valley. The significant variability in the resistivity of the buried rocks of stretch **a** (below the landslide and subglacial sediments) (between 2.2 and 4.0 ohm-metres) is probably due to a variabily fractured bedrock. A band with a minor resistivity (with a range of 110–130 m and a log10 resistivity between 2.2 and 2.8 ohm-metres) indicates a possible buried structure (structure **1**), which is also suggested by the subvertical net surfaces that abruptly border the hard bedrock both to the south and north. This structure (approximately 100 m wide) is a significant element that defines the boundary between gneiss and micaschist. The surficial elongated depression observed in the field (at 215 m progressive) corresponding to a decrease in resistivity, both at the surface (log10 resistivity of 3.2) and at depth (log10 resistivity of 3.0), can be referred to as the subvertical gravitational structure reported as a trench in the geological map (structure **2**).

The high resistivity of the surficial rocks forming stretch **b** (with a range of 250–305 m and a log10 resistivity between 3.6 and 4.0 ohm-metres) is related to a dry bedrock outcrop consisting of gneiss as reported in the geological map (Figure 5). The medium resistivity (between 3.0 and 3.4 ohm-metres) of the shallow subsoil of stretch **b** (from depths of 10

and 20 m) suggests fractured bedrock characterised by higher moisture than the surface rocks. The surficial small NW-SE elongated depression (at 260 m as evidenced in the field) corresponds to an abrupt decrease in resistivity at depth (approximately 30-50 m) which is compatible with a subvertical trench (structure **3**).

The low surficial resistivity of the short stretch **c** (with a range of 305–335 m and a log10 resistivity between 2.0 and 2.6 ohm-metres) is in agreement with the subglacial sediments reported in the geological map (Figure 5). These low values are only broken by a small sector of high resistivity (with a range of 315–325 m and a log10 resistivity between 3.4 and 4.0 ohm-metres) corresponding to the bedrock outcrop reported in the geological map (Figure 5). The high resistivity of the shallow subsoil suggests that the subglacial cover directly lies on coherent bedrock.

The observation that the subglacial sediments partly filled the elongated depression observed in the field (at 330 m) and the sudden occurrence at depth (approximately 30 m) of low-resistivity rocks (values between 2.6 and 2.8 ohm-metres) can be read as evidence of a trench, which is also reported in the geological map (Figure 5) (structure **4**).

A discontinuous thin surficial cover of the high-resistivity rocks of most stretch **d** (with a range of 420–860 m and log10 resistivity between 3.0 and 4.0 ohm-metres) consists of dry sediments rich in clasts. They correspond to debris flows (ranging from 335 to 420 m) and torrential sediments (ranging from 430 to 515 m) forming an alluvial fan (Figure 10), ice-marginal (forming a lateral moraine, ranging from 545 to 615 m, and a frontal moraine, ranging from 780 to 860 m which continues in the stretch **e**) (Figure 11), and landslide deposits (range of 625–705 m) as reported in the geological map. The local medium–low resistivity of the torrential sediments (ranging from 480 to 515 m and from 435 to 445 m) is possibly due to wet conditions along T. Tsa de Fourmière and its small tributary watercourse.

The low resistivity of the surficial level and shallow subsoil (10–20 m deep) of most stretch **d** (with a range of 420–860 m and a log10 resistivity between 2.2 and 3.2 ohm-metres) suggests thick subglacial sediments. The local medium resistivity of the shallow subsoil of the NE sector of stretch **d** (with a range of 335–420 m and a log10 resistivity between 2.8 and 3.4 ohm-metres) can be interpreted as subglacial sediments, whose higher resistivity values than the usual values are due to the location of these sediments sandwiched between the above debris flow and the underlying strong bedrock.

Consequently, the overall distribution and thickness of the subglacial sediments suggest a glacial valley floor that is approximately 500 m wide and bordered by the flanks of the glacial valley shaped in the bedrock (Figure 8A). The abrupt occurrence of low-resistivity rocks up to 50 m deep (at 415 m with a log10 resistivity between 2.8 and 3.6 ohm-metres) can be interpreted as a buried north-facing gravitational structure (structure **5**).

The deep subsoil of stretch **d** is characterised mainly by significant variability in resistivity from very low to medium (with a range of 500–840 m and a log10 resistivity between 2.0 and 3.2 ohm-metres), indicating a variabily fractured bedrock.

The surficial level of low resistivity, typical of subglacial sediments, is locally evident up to a depth of 30 m and lies above lower resistivity rocks (log10 resistivity between 2.0 and 2.8 ohm-metres), which is probably related to bands of very fractured bedrock.

These bands can be related to particularly fractured rocks corresponding to an outcropping gravitational structure (structure **6**) and other buried gravitational structures (structures **7**, **8**, and **9**). These elements involve the bedrock, which shows depressions probably filled by subglacial sediments, resulting in irregularities at the base of the subglacial sediments. These structures have a surficial prolongation towards the SE, forming north-facing and south-facing outcropping scarps that border towards the north the elongated Tsa de Fourmière Relief (TFR) shaped in calcschist. Only the northern side of this stretch has a relatively high resistivity (with a range of 435–490 m and a log10 resistivity between 3.4 and 4.0 ohm-metres), which is probably related to a fractured bedrock.

Figure 10. Torrential sediments forming the alluvial fan (af) of the T. Tsa de Fourmière along the stretch **d** of the ERT1 profile (with a range of 430–460 m). A wide body consisting of debris flow sediments (df) is also evident behind the person.

The surficial high resistivity of stretch **e** (ranging from 860 to 960 m) is related to coarse-grained sediments. These deposits are referred to as ice-marginal sediments, forming a broad ridge corresponding to a significant frontal moraine (Figure 11), and torrential sediments at the end of the profile, related to the alluvial fan of the T. Clapin, as deduced by the geological survey (Figure 5), which lie above a likely poorly fractured hard bedrock.

The band of low resistivity (at 870 m, the log10 resistivity is between 2.4 and 3.0 ohm-metres) can be related to very fractured rocks probably referred to as buried gravitational structures (structure **10**), which are also recognised as outcropping trenches in the ERT2 profile.

The low resistivity of the surficial level and shallow subsoil in the stretch **a** of ERT2 (Figure 8B) corresponding to the two slopes of the Clapin Valley (Figure 12) (with a range of 0–210 m and a log10 resistivity between 2.4 and 3.2 ohm-metres) is in agreement with that of subglacial sediments as evidenced by the geological survey (Figure 5), which is only broken by a high resistivity value (ranging from 75 to 85 m) corresponding to a gneiss outcrop observed in the field. The local surficial level of high resistivity (with a range of 150–210 m and a log10 resistivity between 3.2 and 4.0 ohm-metres) suggests dry clast-rich cover on the subglacial sediments. The geological survey revealed an ice-marginal cover forming a right lateral moraine in the Clapin Valley (Figure 5). The very high resistivity values below a depth of 10–15 m in this first stretch (log10 resistivity between 3.4 and

4.0 ohm-metres) can be attributed to homogeneous hard bedrock probably consisting of gneiss outcropping in the surroundings (Figure 8B).

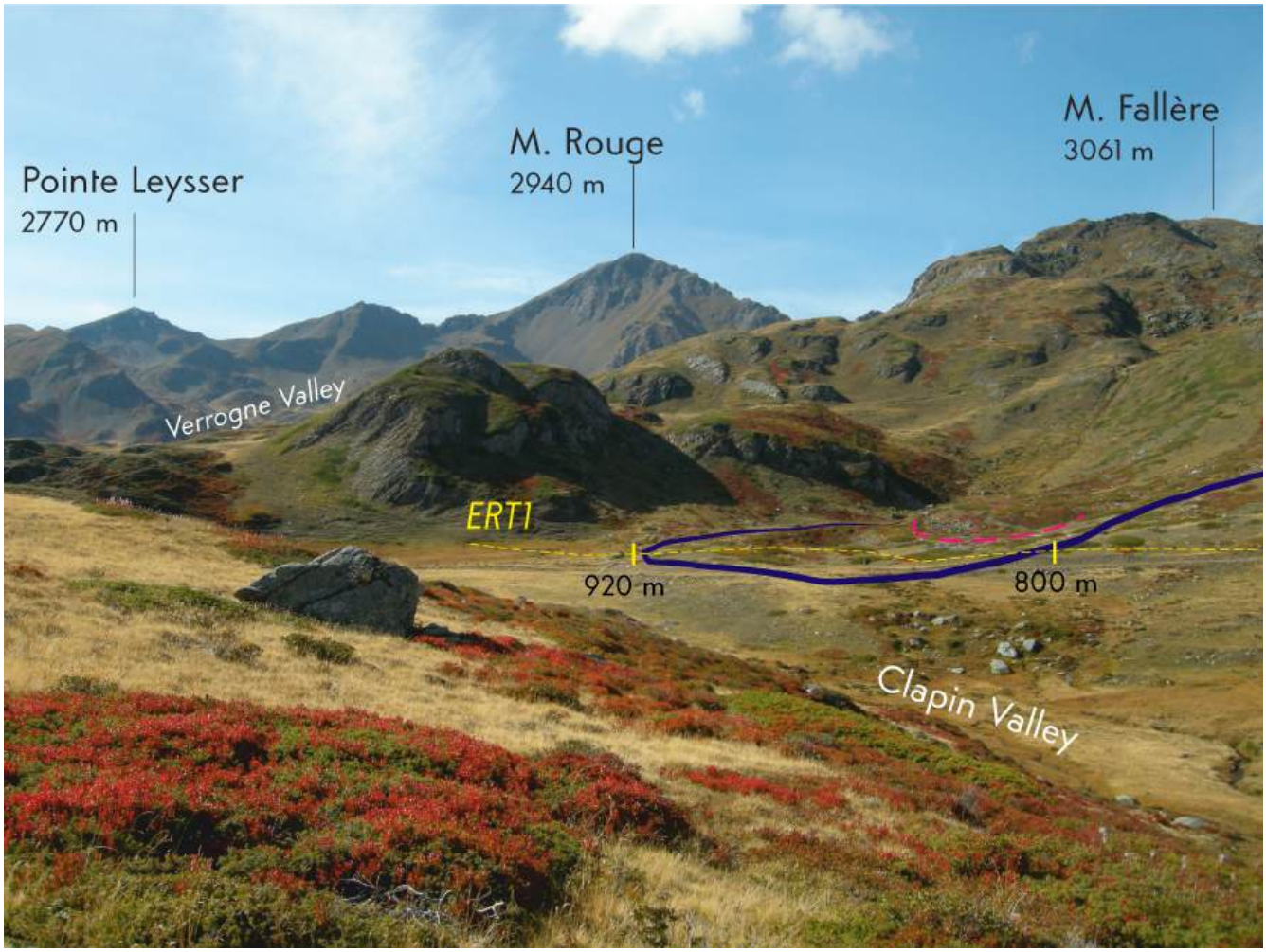

Figure 11. The frontal moraine (light blue line) at the Clapin Valley head along the stretches **d** and **e** of ERT1 (with a range of 800–920 m), formed by ice-marginal sediments, which are partly covered by a landslide body (red dotted line).

Field observations and geophysical data indicate that stretch **a** involves several structures. The sharp increase in the subglacial sediment thickness towards the north (at 45 m, from a few metres to approximately 15 m), in a DSGSD context, suggests that a buried, dipping north, gravitational element (structure **8**) could have displaced the bedrock. This result is more evident in ERT1 than in ERT2. Moreover, another gravitational structure can be hypothesised by the high thickness of the subglacial sediments (approximately 15 m, at 120 m) suggesting a buried trench (structure **10**, also evidenced in ERT1 as a buried structure) (Figure 8A). The subvertical sharp boundary in the subsoil, which abruptly cuts off the hard bedrock to the south, probably represents its extension in depth.

The surficial WNW–ESE north-facing scarp at progressive 165 m (Figure 12) reported in the geological map involving the ice-marginal sediments (Figure 5) correlates in the subsoil (at depths of 10–30 m) to a buried band of low-resistivity rocks (with a range of 160–180 m and a log10 resistivity between 3.0 and 3.4 ohm-metres), suggesting an outcropping gravitational element (structure **11**) (Figure 13).

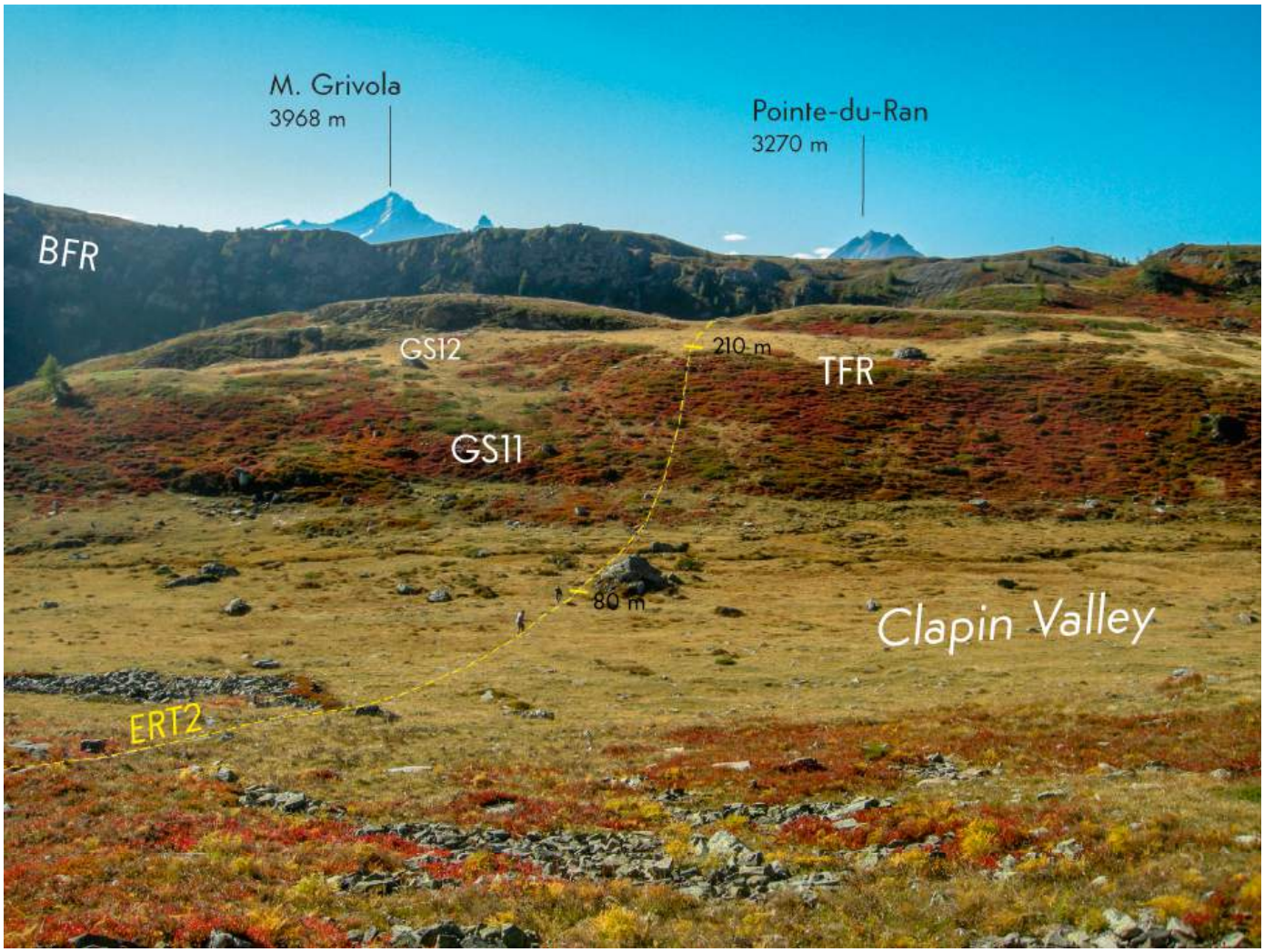

Figure 12. Trend in ERT2 (with a range of 80–210 m) along the Clapin Valley (partially filled by subglacial sediments) bordered by the Tsa de Fourmière Relief (TFR), shaped in the bedrock by subglacial erosion and cut by the gravitational structures **GS11** (scarp on ice-marginal sediments with rhododendrons) and **12** (trench filled by subglacial sediments). In the background, the Becca France ridge (BFR) can be seen.

The high resistivity of the surficial level along stretch **b** corresponding to the northern slope and the summit of the Tsa de Fourmière Relief (with a range of 210–330 m and a log10 resistivity between 3.4 and 4.0 ohm-metres) can be related to dry outcropping bedrock consisting of calcschist, as can be observed in the geological map.

The WNW–ESE elongated depression on the topographic surface (Figure 12), which is partly filled by subglacial sediments and reported as a trench with the same orientation on the geological map, is represented in the profile by a surficial band of sediments with medium resistivity (with a range of 220–230 m and a log10 resistivity between 2.6 and 3.4 ohm-metres). This context correlates in the subsoil with the buried subvertical band of low-resistivity rocks (values between 2.6 and 3.4 ohm-metres), suggesting the presence of very fractured rocks up a depth of 30 m, which longitudinally weakens the relief (structure **12**) (Figure 8B).

Figure 13. Tsa de Fourmière Relief (TFR) shaped in the bedrock by subglacial erosion and cut by the WNW–ESE gravitational minor scarp (**GS11**, with a height of 15–20 m) east of the ERT2 profile. In the background, the summit of the Becca France ridge is visible.

Other WNW–ESE surficial wide elongated depressions, also referred to as trenches in the geological map, filled by a thin body of subglacial sediments, correlate in the subsoil with the two evident buried subvertical bands of low-resistivity rocks (with ranges of 270–280 and 290–295 m, respectively, and log10 resistivity values between 2.0 and 3.2 ohm-metres) at the depths of approximately 10–40 m that reveal gravitational elements (structures **13** and **14**) (Figure 14). The southern structure (structure **14**) even represents the boundary between the outcropping carbonate-rich calcschist and dolomitic marble, as evidenced by the geological survey (Figure 5).

The low resistivity of the surficial level and the shallow subsoil detected along stretch **c** (with a range of 330–540 m and a log10 resistivity between 2.4 and 3.0 ohm-metres), corresponding to the southern slope of the Tsa de Fourmière Relief and the head of the Clusellaz Valley indicates the wide distribution of subglacial sediments. The subglacial body is covered at both ends of this range by a thin level of dry clast-rich deposits with high resistivity (with ranges of 330–370 m and 460–540 m and log10 resistivity values between 3.2 and 4.0 ohm-metres). This context suggests the presence of debris (at the northern end) and ice-marginal sediments forming the three left lateral–frontal moraines (at the southern end) (Figure 6) reported in the geological map in the Clusellaz Valley (Figure 5). The high thickness of sediments (10–30 m) showing low resistivity in this range of the profile suggests a significant thickness of subglacial sediments that can be explained by a

wide and deep buried glacial valley shaped in the bedrock. The medium resistivity (log10 resistivity between 2.6 and 3.6) of the rocks underlying the subglacial cover in this range may be related to highly fractured bedrock (Figure 15).

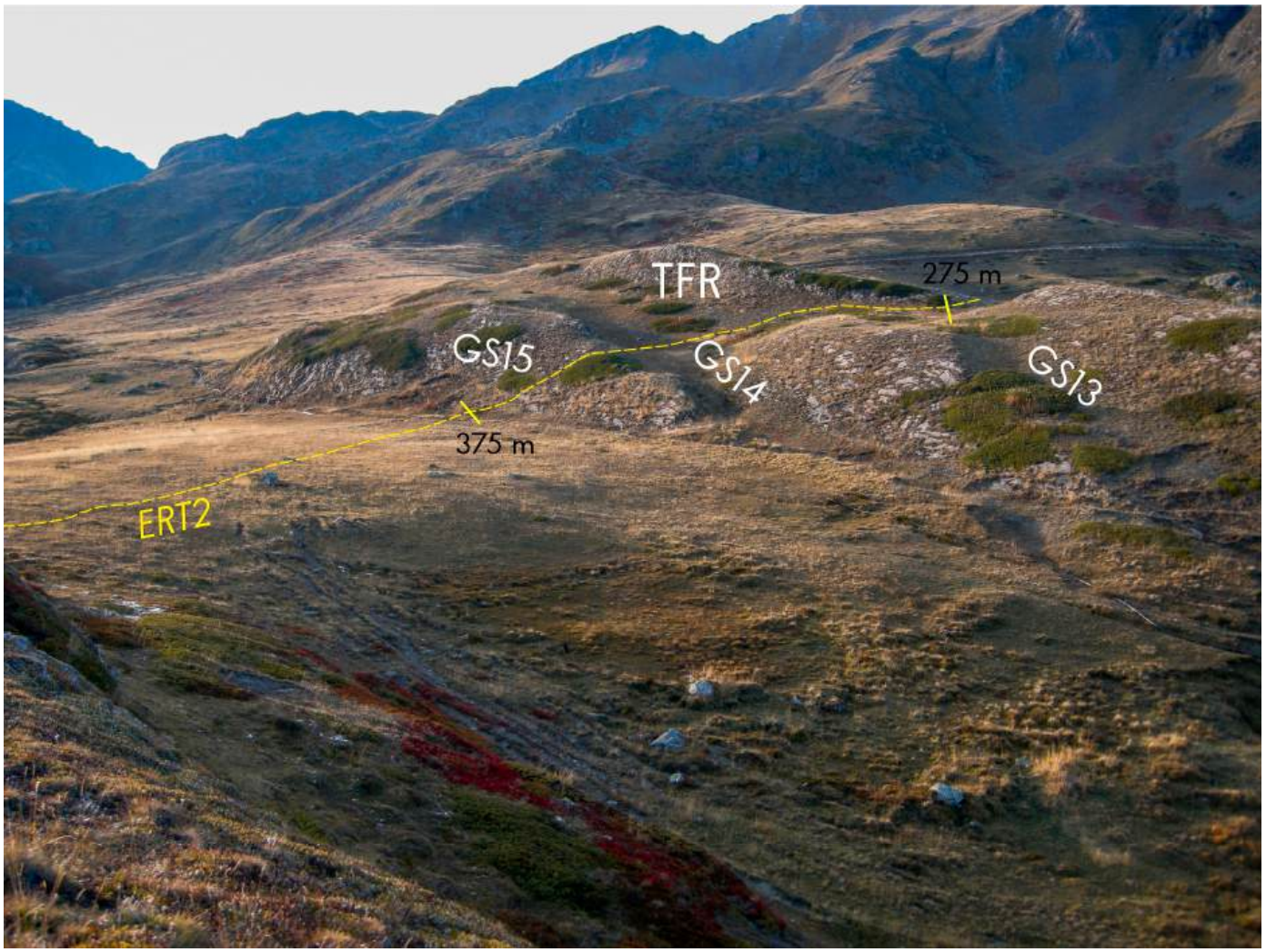

Figure 14. Gravitational trenches (**GS13** and **GS14**) and minor scarps (**GS15**) along stretch **b** of the ERT2 profile (with a range of 275–375 m) cut the Tsa de Fourmière Relief (TFR) shaped in the bedrock by subglacial erosion.

Stretch **c** is bounded towards the north by the high-resistivity outcropping calcschist of the Tsa de Fourmière Relief (TFR) (with a range of 310–330 m and a log10 resistivity between 3.2 and 4.0 ohm-metres) and towards the south by the medium–high resistivity of the buried bedrock of the northern slope of the Becca France ridge (with a range of 540–570 m and a log10 resistivity between 2.6 and 4.0 ohm-metres). This buried glacial valley shaped in the fractured bedrock is laterally bounded by two gravitational surfaces (a southern-dipping element and an opposite northern-dipping element), both of which correspond to the significant jumps of resistivity (at 340 and 540 m, respectively) (structures **15** and **19**) (Figure 14). The WNW–ESE 10 m high wall, referred to as the southwards-dipping scarp in the geological map, represents the surficial evidence of the first jump in resistivity (structure **15**). In contrast, the second structure (structure **19**) can be explained by a gravitational element buried by the ice-marginal sediments.

Three bands in which the low resistivity is particularly thick in the shallow subsoil are detected in the profile (at 410, 460, and 490 m, the log10 resistivity is between 2.2 and 2.8 ohm-metres), suggesting various thicknesses of the subglacial sediments that fill the

irregularities of the glacial valley rocky floor up to 40 m. These bands are likely to be explained as locally buried elongated depressions in the fractured bedrock connected to gravitational structures (at ranges 400–405, 460–465, and 490–495 m, structures **16**, **17**, and **18**) which conditions the thickness of glacial sediments.

Figure 15. Persistent joints feature the high fractured rocks (calcschist) outcropping in the Tsa de Fourmière Relief (TFR) (approximately 20 m high).

The stretch **d** (ranging from 540 to 710 m) is composed of two parts: the valley floor of the Clusellaz Valley and the northern side of the Becca France ridge. The average surficial high resistivity of the northern slope of Becca France (corresponding to the right side of the Clusellaz Valley) in this stretch (with a range of 570–620 m and a log10 resistivity between 3.4 and 4.0 ohm-metres) is in agreement with dry clast-rich deposits. They can be referred to as the ice-marginal sediments that form the more internal right lateral–frontal moraine reported in the geological map (Figure 3). The low resistivity along the torrential valley floor of the Clusellaz Valley (with a range of 540–570 m and a log10 resistivity between 2.4 and 2.8 ohm-metres) may be related to the high soil moisture of these surficial sediments along the watercourse. The medium resistivity of the next stretch (with a range of 620–670 m and a log10 resistivity between 3.0 and 3.4 ohm-metres) even suggests ice-marginal sediments. The medium resistivity is related to the flat morphology of the summit of another right lateral–frontal moraine. The lack of low-resistivity rocks below these bodies suggests that the ice-marginal sediments lie directly on the bedrock and are characterised by a medium to high resistivity (log10 resistivity between 2.8 and 4.0 ohm-metres). This bedrock shows two bands of medium resistivity (at 610 and 630 m, the log10 resistivity is between 2.4 and 3.2 ohm-metres), indicating buried gravitational structures (structures **20** and **21**) (Figure 6). They consist of north-dipping elements that extend from the outcropping north-facing

scarps reported immediately to the west of the profile in the geological map. Additionally, the medium–high resistivity of the southern end of the profile (with a range of 670–710 m and a log10 resistivity between 3.0 and 3.6 ohm-metres) is compatible with bedrock. This bedrock shows that a band of medium resistivity (at 680 m, the log10 resistivity is between 2.6 and 3.0 ohm-metres), which is in agreement with outcropping south-facing scarps, located immediately east and west of the profile, can be related to a dip towards the south element.

6. Discussion

The interpretation criteria applied to these ERT profiles are coherent with those reported by several literature studies, which adopt the same technique in DSGSD environments. In particular, ERT has already demonstrated its ability to identify subvertical low-resistivity bands, which are usually related to trenches or faults, e.g., [18], or the shallow horizontal contrast between the high-resistivity cover and low-resistivity underlying rocks, which is usually related to a change in saturation, e.g., [20], or to the presence of shallow coarse-grained sediments, e.g., [18]. Notably, the effects of subvertical structures such as those identified in the present study, on ERT profiles have been widely discussed, with direct forward the analyses of simulated models, e.g., [15]. These simulations depict a resulting resistivity distribution of the ERTs consistent with what is reported in the present paper, allowing us to ascertain the presence of these structures with a high degree of confidence.

The influence of lateral rocks (i.e., 3D effects) cannot be neglected when interpreting very long ERT profiles, especially for increasing distances between current injection electrodes. To better interpret the lateral structure effect, we tested a 3D inversion via the same ResIPy inversion algorithm. An example result of the 3D inversions is reported (Figure 16).

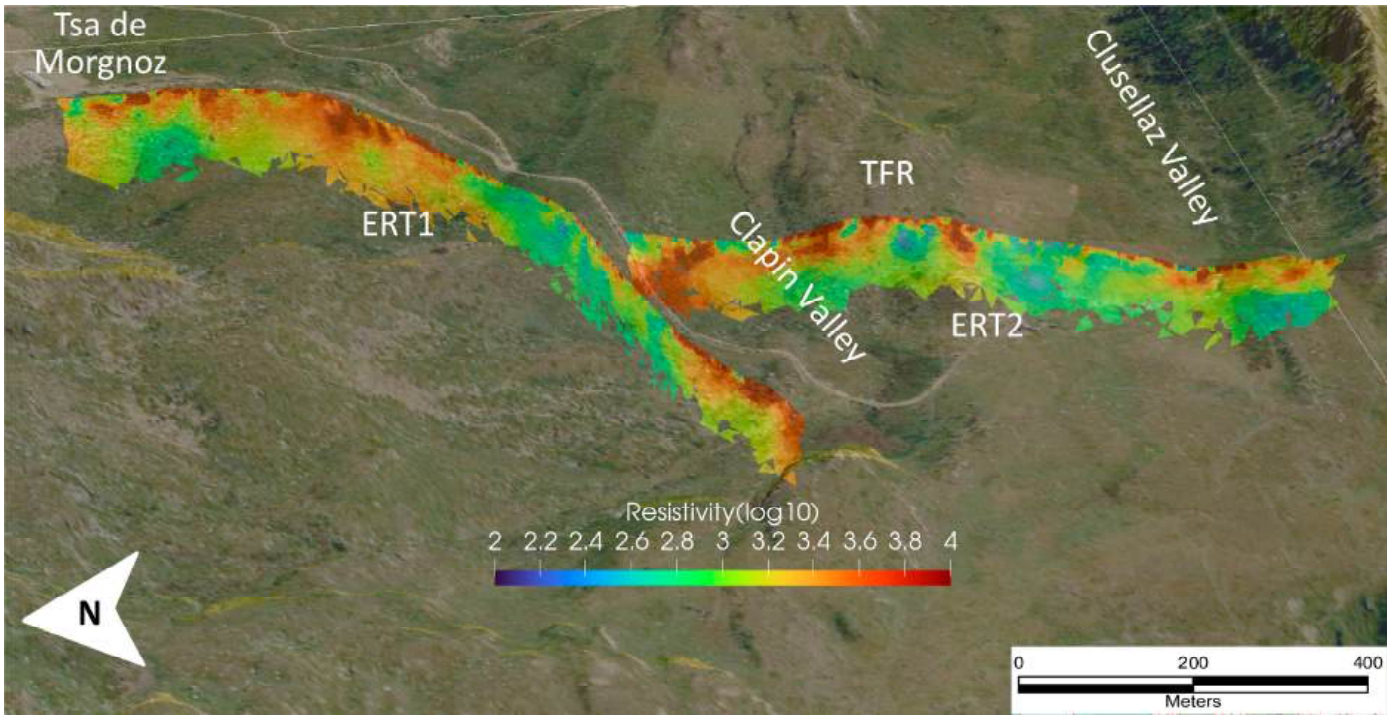

Figure 16. The 3D visualisation of the 3D inversion of the two ERT profiles seen from the NW. The Y axis indicates the north direction.

However, no particular improvements or differences can be noted compared with the 2D results, probably because the chosen survey directions were selected to cut the structures visible on the surface almost perpendicularly. In this context, 3D effects along the profiles

should be considered of minor relevance. The 3D inversion and georeferencing of ERT data is, nevertheless, a valuable tool for visualising resistivity models in a 3D environment composed of an orthophoto and a digital elevation model, as shown in Figure 16.

The two geophysical profiles involve the southern slope of Mont Fallère. It is drained by two small tributaries of the Fallère Valley (T. Tsa de Morgnoz and T. Tsa de Fourmière) and by the greater Clapin and Clusellaz torrents (Figure 3). The tributary watercourses have a NNW–SSE trend orientation, which is the direction of the maximum slope. In contrast, the Clapin and Clusellaz torrents show an anomalous WNW-ESE orientation parallel to the Becca France ridge. The Clapin (Figure 17) and Tsa de Fourmière torrents flow into a wide valley furrow shaped in the bedrock, which is partially filled by glacial deposits, suggesting that it corresponds to a significant glacial valley (glacial Clapin Valley). The T. Clusellaz flows in another depression (glacial Clusellaz Valley). In contrast, the T. Tsa de Morgnoz flows on a rocky slope shaped by areal subglacial erosion. A rocky relief, several tens of metres high and parallel to the valleys, has undergone subglacial erosion (Tsa de Fourmière Relief, TFR) and separates the two glacial Clapin and Clusellaz Valleys.

Field observations allow only a partial understanding of the geological setting, whose full comprehension also requires geophysical investigations to add information for the shallow subsoil.

The main general results for the investigated area, combining geological and geophysical surveys, are reported below.

- The presence of rocks or sediments with different resistivity values near the surface confirms the data inferred from the geological survey. The stretches showing high resistivity at both the surface and depth consist of bedrock. The stretches with high resistivity values only at the surface represent sectors where permeable and dry clast-rich deposits (ice-marginal, torrential, landslide, and debris flow) outcrop. Stretches with low resistivity values at the surface or shallow subsoil are related to sectors shaped in fine and impermeable deposits (e.g., subglacial).
- The outcropping gravitational structures that displace bedrock and Quaternary cover and landforms (detected by field observations) usually continue at depth, as evidenced by bands of reduced resistivity.
- Similarly, the deep bands of low resistivity indicate the extent in depth of structures (gravitational or tectonic) not detectable by field surveys, as their morphology has been erased by subglacial abrasion or covered by Quaternary sediments.
- The investigated area is cut by three great WNW–ESE glacial valleys (Tsa de Morgnoz, Clapin, and Clusellaz) (Figure 17) with wide widths (between 200 and 500 m), which are only partly evident in the field observations because they are filled by subglacial deposits locally covered by ice-marginal and other sediments. Geophysical investigations highlighted a significant depth of the bedrock floor (up to 30–40 m). The morphological evidence of these valleys is hidden (particularly for the Tsa de Morgnoz and Clapin Valleys).
- The same geophysical investigations indicate that glacial valley floors are shaped on large bands of highly fractured bedrock bounded by slopes shaped in more competent bedrock. The abrupt change in the degree of fracturing in the bedrock is in agreement with the occurrence of WNW–ESE gravitational structures. This arrangement, particularly evident for the Clusellaz Valley, where the structures converge towards the centre of the morphological incision, suggests that this valley is set along graben-like structures, indicative of extension phenomena. These phenomena agree with the strain analysis in the surrounding area, which reveals incremental strain axes in the NE–SW extensional direction during the Oligocene–present time span [51].

Figure 17. The glacial Clapin Trough (approximately 40 m wide), east of the ERT2 profile, is partly filled by subglacial sediments, as evidenced by wide meadows.

Geophysical investigations have also shown that the Tsa d Morgnoz, Clapin, and Clusellaz wide glacial valleys have irregular floors due to the presence of several troughs, filled with subglacial sediments, which are relatively deep (up to 30/40 m) and set along narrow, very fractured bedrock bands (up to several tens of metres wide). These irregularities of glacial valley floors and other covered elements correspond to buried gravitational structures. Gravitational structures evolved partly earlier than the last glacial expansion, influencing the glacial shaping of these valleys.

Moreover, the outcropping gravitational structures evidenced by field surveys are in agreement with the subsequent postglacial gravitational evolution (Figure 18). Some of these outcropping elements may be older gravitational structures whose primary morphological expression has been abraded by glaciers. In these cases, the current evidence is related to recent gravitational evolution.

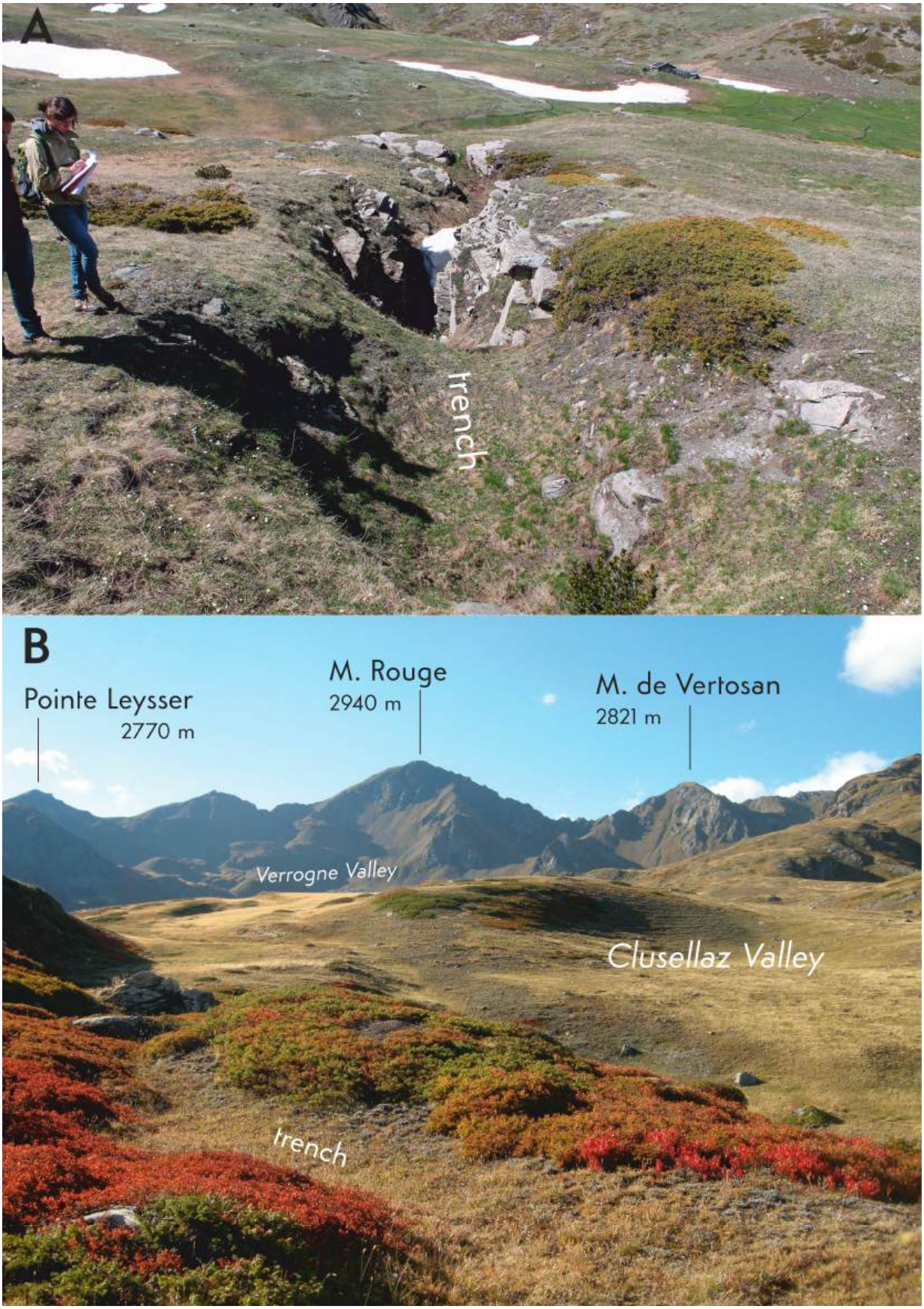

Figure 18. Trench west of the ERT2 profile: (**A**) stretch of this trench shaped in the bedrock and (**B**) stretch of this trench (approximately 3 m wide) involving the subglacial sediments.

Previous regional geological data indicate the presence, in the NE sector of the ERT1 profile, of the tectonic boundary between two important geological units (the Mont Fort Unit and Aouilletta Unit) separated by the Chaligne Fault System [56,60]. The same data suggest that the displacement along this structure is difficult to evaluate for the occurrence of a large DSGSD that hinders direct observation [51]. Our detailed field data indicate the presence, in the same sector, of the buried boundary between gneiss and micaschist referred to as the Mont Fort Unit. The presence of a discontinuity in the bedrock, evidenced by geophysical investigation, is shown by a large rock band of medium to high fracturing degree. The possibility of attributing this band to tectonic or gravitational phenomena is uncertain. However, the observation that this structure can be followed laterally for more than a dozen kilometres agrees with the partial tectonic origin of this system [60]. According to the field survey, both the morphological depressions and reliefs and the gravitational structures have a setting approximately parallel to the trend in the Chaligne System. This setting suggests that the recognised gravitational structures could have evolved along ancient tectonic structures.

More generally, the investigated area represents a wide asymmetrical depression showing a high left slope (southern Mont Fallère slope) characterised by a WNW–ESE watershed with high peaks (Mont Fallère, 3061 m; Mont d'Ars, 2826 m; Mont de La Tza, 2741 m) and a right low slope, which shows, on the contrary, a NW–SE watershed corresponding to a lower ridge (Becca France, 2312–2347 m) (Figure 2). Consequently, the two sides have different slopes, with a higher left side.

This setting represents the main geological evidence that the studied area is not a simply glacial landform (abraded by glaciers) but consists of a gravitational valley [46] connected to a lowering and distancing between the two sides (namely, the southern side of Mont Fallère and the northern side of Becca France), subsequently shaped by glaciers and watercourses. This gravitational landform is mainly set along a broad band of fractured rocks connected to DSGSD movements.

7. Conclusions

The geophysical survey results generally confirm the surface features deduced from the new geological survey. The different types of sediments (rich or poor in clasts) reported in the geological map are evidenced by different and specific resistivity values in geophysical profiles. Substantial variations in the resistivity values of the rocks along the geophysical profiles also reveal various degrees of bedrock fracturing. Finally, the presence and location of outcropping gravitational structures, recognised by geological surveys, are usually confirmed by geophysical investigations. These investigations also made it possible to refine the surficial geological setting locally, where natural phenomena or anthropogenic interventions reshape the primary morphological evidence of sediments.

The recognition of buried elements through geophysical investigations has greatly enhanced the mapping of surficial bedrock, sediments and structures. For example, three wide glacial valleys (Clusellaz, Clapin, and Morgnoz) are recognised, which are set along the hectometric bands of significantly fractured bedrock and are partly filled by subglacial sediments. Their partial filling, which modified the morphology, has led to a present-day hydrographic network that does not fully follow the previous glacial flow lines.

Moreover, geophysical investigations define the continuation of several surficial structures in shallow and deeper subsoil. In addition, these investigations also provide evidence of buried structures that lack surficial morphological evidence.

The geological framework resulting from all the performed observations (field and geophysical data) reveals an area intensely deformed by extensional gravitational movements in a predominantly NE–SW direction. These movements involve a sector already affected by previous tectonic movements related to the Chaligne Fault System.

The combination of outputs derived from field surveys and geophysical techniques also allows us to evaluate the temporal relationship between glacial shaping and gravitational evolution. Bands of very fractured bedrock buried by glacial deposits are interpreted

as older gravitational structures that evolved before the Last Glacial Maximum and were not subsequently reactivated. The structures that dislocate glacial deposits and landforms indicate, on the contrary, a postglacial evolution.

The reading of the geological setting in the study area can provide an overall understanding of the anomalous trend in the glacial Clapin and Clusellaz Valleys and Becca France ridge, characterised by an orientation subparallel to the central Dora Baltea Valley. These valleys, described by geophysical investigations as having a band of very fractured bedrock, can be interpreted as evidence of wide and articulated gravitational valleys.

The results of the geological setting and the specific geophysical surveys in the investigated area allow a first interpretation of the anomalous trend in the Becca France ridge and the glacial Clapin and Clusellaz Valleys, characterised by an orientation subparallel to the central Dora Baltea Valley. Indeed, geophysical investigations indicate that these valleys develop along the bands of extremely fractured bedrock, which suggests the presence of broad and well-articulated gravitational valleys. Further geophysical surveys are recommended in the other sectors of the western Alps, applying the same methodology used in this work, essentially to better evaluate the buried gravity-induced structures.

Author Contributions: Conceptualization, M.G.F., M.G. and C.C.; methodology, F.G.; software, A.V. and S.D.; vali-dation, M.G.F., M.G., F.G. and C.C.; formal analysis, C.C., A.V. and S.D.; investigation, C.C., A.V. and S.D.; resources, S.D.; data curation, F.G.; writing—original draft preparation, M.G.F., M.G. and F.G.; writing—review and editing, M.G.F., M.G. and F.G.; visualization, S.D.; supervision, M.G.F., M.G. and C.C.; project administration, M.G.F. and M.G.; funding acquisition, M.G.F. and M.G. All authors have read and agreed to the published version of the manuscript.

Funding: The project was supported by the University of Torino ("Ricerca Locale ex 60% 2022 and 2023", grants to A. Festa), the Italian Ministry of University and Research ('Cofin-PRIN 2020 "POEM project—POligEnetic Mélanges: anatomy, significance and societal impact", grants n° 2020542ET7_003 to A. Festa).

Data Availability Statement: The raw and processed data of the ERT survey were made openly available for inspection and reuse on a Zenodo repository, accessible at the link https://zenodo.org/doi/10.5281/zenodo.12579207.

Acknowledgments: A special thanks to Diego Franco for his help with instrumentation and fieldwork.

Conflicts of Interest: The authors declare no conflict of interest.

References

1. Alexandrowicz, Z.; Alexandrowicz, S.W. Ridge top trenches and rifts in the Polish Outer Carpathians. *Ann. Soc. Geol. Pol.* **1988**, *58*, 207–228.
2. Calò, F.; Ardizzone, F.; Castaldo, R.; Lollino, P.; Tizzani, P.; Guzzetti, F.; Lanari, R.; Angeli, M.G.; Pontoni, F.; Manunta, M. Enhanced landslide investigations through advanced DInSAR techniques: The Ivancich case study, Assisi, Italy. *Remote Sens. Environ.* **2014**, *142*, 69–82. [CrossRef]
3. Drouillas, Y.; Lebourg, V.; Zerathe, V.; Hippolyte, J.C.; Chochon, R.; Vidal, M.; Besso, R. Alpine deep-seated gravitational slope deformation and the Messinian Salinity Crisis. *Landslides* **2021**, *18*, 539–549. [CrossRef]
4. Gutiérrez, F.; Linares, R.; Roqué, C.; Zarroca, M.; Rosell, J.; Galve, J.P.; Carbonell, D. Investigating gravitational grabens relatedto lateral spreading and evaporite dissolution subsidence by means of detailed mapping, trenching, and electrical resistivity tomography (Spanish Pyrenees). *Lithos* **2012**, *4*, 331–353. [CrossRef]
5. Herrera, G.; Gutiérrez, F.; García-Davalillo, J.C.; Guerrero, J.; Notti, D.; Galve, J.P.; Fernadez-Merodo, J.A.; Cooksley, G. Multi-sensor advanced DInSAR monitoring of very slow landslides: The Tena Valley case study (Central Spanish Pyrenees). *Remote Sens. Environ.* **2013**, *128*, 31–43. [CrossRef]
6. Hippolyte, J.C.; Brocard, G.; Tardy, M.; Nicoud, G.; Bourlès, D.; Braucher, R.; Ménard, G.; Souffaché, B. The recent fault scarps of the Western Alps (France): Tectonic surface ruptures or gravitational sackung scarps? A combined mapping, geomorphic, and 10Be levelling, and dating approach. *Tectonophysics* **2006**, *418*, 255–276. [CrossRef]
7. Hippolyte, J.C.; Bourlès, D.; Léanni, L.; Braucher, R.; Chauvet, F.; Lebetard, A.E. 10Be ages reveal >12 ka of gravitational movement in a major sackung of the Western Alps (France). *Geomorphology* **2012**, *171–172*, 139–153. [CrossRef]
8. Mantovani, M.; Bossi, G.; Marcato, G.; Schenato, L.; Tedesco, G.; Titti, G.; Pasuto, A. New perspectives in landslide displacement detection using Sentinel-1 datasets. *Remote Sens.* **2019**, *11*, 2135. [CrossRef]

9. Pánek, T.; Hradecký, J.; Šilhán, K.; Smolková, V.; Altová, V. Time constraints for the evolution of a large slope collapse in karstified mountainous terrain (case study from the southwestern tip of the Crimean Mountains, Ukraine). *Geomorphology* **2009**, *108*, 171–181. [CrossRef]
10. Solari, L.; Del Soldato, M.; Montalti, R.; Bianchini, S.; Raspini, F.; Thuegaz, P.; Bertolo, D.; Tofani, V.; Casagli, N. A Sentinel-1based hotspot analysis: Landslide mapping in north-western Italy. *Int. J. Remote Sens.* **2019**, *40*, 7898–7921. [CrossRef]
11. Zerathe, S.; Lebourg, T. Evolution stages of large deep-seated landslides at the front of a subalpine meridional chain (Maritime-Alps, France). *Geomorphology* **2012**, *138*, 390–403. [CrossRef]
12. Dolce, S.; Forno, M.G.; Gattiglio, M.; Gianotti, F. The Lac Fallère as an example of interplay between deep-seated gravitational slope deformation and glacial shaping (Aosta Valley). *GeoHazards* **2024**, *5*, 38–63. [CrossRef]
13. Schrott, L.; Sass, O. Application of field geophysics in geomorphology: Advances and limitations exemplified by case studies. *Geomorphology* **2008**, *93*, 55–73. [CrossRef]
14. Jongmans, D.; Bièvre, G.; Renalier, F.; Schwartz, S.; Beaurez, N.; Orengo, Y. Geophysical investigation of a large landslide in glaciolacustrine clays in the Trièves area (Frech Alps). *Eng. Geol.* **2009**, *109*, 45–56. [CrossRef]
15. Jomard, T.; Lebourg, Y.; Guglielmi, E. Tric Electrical imaging of sliding geometry and fluids associated with a deep seated landslide (La Clapière, France). *Earth Surf. Process. Landf.* **2010**, *35*, 588–599. [CrossRef]
16. Lebourg, M.; Hernandez, S.; Zerathe, S.; El Bedoui, H.; Jomard, B.; Fresia, B. Landslides triggered factors analysed by time lapse electrical survey and multidimensional statistical approach. *Eng. Geol.* **2010**, *114*, 238–250. [CrossRef]
17. Comina, C.; Forno, M.G.; Gattiglio, M.; Gianotti, F.; Raiteri, L.; Sambuelli, L. ERT geophysical surveys contributing to the reconstruction of the geological landscape in high mountain prehistorical archaeological sites (Plan di Modzon, Aosta Valley, Italy). *Ital. J. Geosci.* **2015**, *134*, 95–103. [CrossRef]
18. Chalupa, V.; Pánek, T.; Táborík, P.; Klimeš, J.; Hartvich, F.; Grygar, R. Deep-seated gravitational slope deformations controlled by the structure of flysch nappe outliers: Insights from large-scale electrical resistivity tomography survey and LiDAR mapping. *Geomorphology* **2018**, *321*, 174–187. [CrossRef]
19. Chalupa, V.; Pánek, T.; Šilhán, K.; Březný, M.; Tichavský, R.; Grygar, R. Low-topography deep-seated gravitational slope deformation: Slope instability of flysch thrust fronts (Outer Western Carpathians). *Geomorphology* **2021**, *389*, 107833. [CrossRef]
20. Kasprzak, M.; Jancewicz, K.; Różycka, M.; Kotwicka, W.; Migoń, P. Geomorphology- and geophysics-based recognition of stages of deep-seated slope deformation (Sudetes, SW Poland). *Eng. Geol.* **2019**, *260*, 105230. [CrossRef]
21. Dramis, F.; Sorriso-Valvo, M. Deep-seated gravitational slope deformations, related landslides and tectonics. *Eng. Geol.* **1994**, *38*, 231–243. [CrossRef]
22. Agliardi, F.; Crosta, G.B.; Frattini, P. Slow rock-slope deformation. In *Landslides Types, Mechanisms and Modeling*; Clague, J.J., Stead, D., Eds.; Cambridge University Press: Cambridge, UK, 2012; pp. 207–221. [CrossRef]
23. Crosta, G.; Frattini, P.; Agliardi, F. Deep seated gravitational slope deformations in the European Alps. *Tectonophysics* **2013**, *605*, 13–33. [CrossRef]
24. Zischinsky, U. On the deformation of high slopes. In Proceedings of the Last Conference International Society Rock Mechanics, Lisbon, Portugal, 25 September–1 October 1966; Volume 2, pp. 179–185.
25. Němčok, A. Gravitational slope deformation in high mountains. In Proceedings of the 24th International Geological Congress, Montreal, Canada, 21–30 August 1972; Volume 13, pp. 132–141.
26. Malgot, J. Deep-seated gravitational slope deformations in neovolcanic mountain ranges of Slovakia. *Bull. Eng. Geol. Environ.* **1977**, *16*, 106–109. [CrossRef]
27. Mortara, G.; Sorzana, P.F. Fenomeni di deformazione gravitativa profonda nell'arco alpino occidentale italiano; considerazioni lito-strutturali e morfologiche. *Ital. J. Geosci.* **1987**, *106*, 303–314.
28. Agliardi, F.; Crosta, G.B.; Zanchi, A.; Ravazzi, C. Onset and timing of deep-seated gravitational slope deformations in the eastern Alps, Italy. *Geomorphology* **2009**, *103*, 113–129. [CrossRef]
29. Fioraso, G.; Baggio, P.; Bonadeo, L.; Brunamonte, F. Post-glacial evolution of gravitational slope deformations in the upper Susa and Chisone Valleys (Italian Western Alps). *Ital. J. Quat. Sci.* **2011**, *24*, 104–106.
30. Forno, M.G.; Gattiglio, M.; Gianotti, F.; Rossato, S.; Taddia, G. Deep-seated gravitational slope deformation effects on Quaternary deposits in the western Alps (NW Italy). *Alp. Mediterr. Quat.* **2020**, *33*, 43–60. [CrossRef]
31. Shroder, J.F.; Owen, A.; Seong, Y.B.; Bishop, M.P.; Bush, A.; Caffee, M.C.; Copland, L.; Finkel, R.C.; Kamp, U. The role of mass movements on landscape evolution in the Central Karakoram: Discussion and speculation. *Quat. Int.* **2011**, *236*, 34–47. [CrossRef]
32. Jarman, D.; Calvet, M.; Corominas, J.; Delmas, M.; Gunnell, Y. Large-scale rock slope failures in the eastern Pyrenees: Identifying a sparse but significant population in paraglacial and parafluvial contexts. *Geogr. Ann. Ser. A Phys. Geogr.* **2014**, *96*, 357–391. [CrossRef]
33. Agliardi, F.; Crosta, G.B.; Frattini, P.; Malusà, M.G. Giant non-catastrophic landslides and the long-term exhumation of the European Alps. *Earth Planet. Sci. Lett.* **2013**, *365*, 263–274. [CrossRef]
34. Martinotti, G.; Giordan, D.; Giardino, M.; Ratto, S. Controlling factors for deep-seated gravitational slope deformation (DSGSD) in the Aosta Valley (NW Alps, Italy). *Geol. Soc. Lond. Spec. Publ.* **2011**, *351*, 113–131. [CrossRef]
35. Ambrosi, C.; Crosta, G.B. Large sackung along major tectonic features in the Central Italian Alps. *Eng. Geol.* **2006**, *83*, 183–200. [CrossRef]

36. Esposito, C.; Di Luzio, E.; Baleani, M.; Troiani, F.; Della Seta, M.; Bozzano, F.; Mazzanti, P. Fold architecture predisposing deep-seated gravitational slope deformations within a flysch sequence in the Northern Apennines (Italy). *Geomorphology* **2021**, *380*, 107629. [CrossRef]
37. Gori, S.; Falcucci, E.; Dramis, F.; Galadini, F.; Galli, P.; Giaccio, B.; Messina, P.; Pizzi, A.; Sposato, A.; Cosentino, D. Deep-seated gravitational slope deformation, largescale rock failure, and active normal faulting along Mt. Morrone (Sulmona basin, central Italy): Geomorphological and paleoseismological analyses. *Geomorphology* **2014**, *208*, 88–101. [CrossRef]
38. Moro, M.; Saroli, M.; Gori, S.; Falcucci, E.; Galadini, F.; Messina, P. The interaction between active normal faulting and large-scale gravitational mass movements revealed by paleoseismological techniques: A case study from central Italy. *Geomorphology* **2012**, *151–152*, 164–174. [CrossRef]
39. Fioraso, G. Impact of massive deep-seated rock slope failures on mountain valley morphology in the northern Cottian Alps (NW Italy). *J. Maps* **2017**, *13*, 575–587. [CrossRef]
40. Cody, E.; Anderson, B.M.; McColl, S.T.; Fuller, I.C.; Purdie, H.L. Paraglacial adjustment of sediment slopes during and immediately after the debuttressing. *Geomorphology* **2020**, *371*, 107411. [CrossRef]
41. Mantovani, M.; Bossi, G.; Dykes, A.; Pasuto, A.; Soldati, M.; Devoto, S. Coupling long-term GNSS monitoring and numerical modelling of lateral spreading for hazard assessment purposes. *Eng. Geol.* **2022**, *296*, 106466. [CrossRef]
42. Cignetti, M.; Manconi, A.; Manunta, M.; Giordan, D.; De Luca, C.; Allasia, P.; Ardizzone, F. Taking advantage of the ESA G-POD service to study ground deformation processes in high mountain areas: A Valle d'Aosta case study, Northern Italy. *Remote Sens.* **2016**, *8*, 852. [CrossRef]
43. Agliardi, F.; Crosta, G.; Zanchi, A. Structural constraints on deep-seated slope deformation kinematics. *Eng. Geol.* **2001**, *59*, 83–102. [CrossRef]
44. Dal Piaz, G.V. *Guide Geologiche Regionali, Le Alpi dal Monte Bianco al Lago Maggiore, Parte Prima*; BE-MA Editrice: Milan, Italy, 1992.
45. Pánek, T.; Klimeš, J. Temporal behavior of deep-seated gravitational slope deformations: A review. *Earth Sci. Rev.* **2016**, *156*, 14–38. [CrossRef]
46. Forno, M.G.; Gattiglio, M.; Ghignone, S.; Taddia, G. Deep-seated gravitational slope deformation involving glacial evidence in the Rodoretto Valley (NW Alps). *J. Maps* **2021**, *17*, 846–858. [CrossRef]
47. Forno, M.G.; Comina, C.; Gattiglio, M.; Gianotti, F.; Lo Russo, S.; Sambuelli, L.; Raiteri, L.; Taddia, G. Preservation of Quaternary sediments in DSGSD environment: The Mont Fallère case study (Aosta valley, NW Italy). *Alp. Mediterr. Quat.* **2016**, *29*, 181–191. Available online: https://amq.aiqua.it/index.php/amq/article/view/104 (accessed on 18 October 2021).
48. Forno, M.G.; Bollati, I.M.; Gattiglio, M.; Gianotti, F.; Pelfini, M.; Sartori, G. How can a complex geosite be enhanced? A landscape-scale approach at the Deep Seated Gravitational Slope Deformation of Pointe Leysser (Aosta Valley, NW Italy). *Geoheritage* **2022**, *14*, 100. [CrossRef]
49. Forno, M.G.; Fubelli, G.; Gattiglio, M.; Taddia, G.; Ghignone, S. Object-based geomorphological mapping: Application on an Alpine deep-seated gravitational slope deformation contest (Germanasca Valley, Western Alps). *Appl. Sci.* **2022**, *12*, 778. [CrossRef]
50. Delle Piane, L.; Perello, P.; Baietto, A.; Giorza, A.; Musso, A.; Gabriele, P.; Baster, I. Mature vs. active deep-seated landslides: A comparison through two case histories in the Alps. *Rock Mech. Rock Eng.* **2016**, *49*, 2189–2216. [CrossRef]
51. Ratto, S.; Giardino, M.; Giordan, D.; Alberto, W.; Armand, M. *Carta dei Fenomeni Franosi della Valle d'Aosta, 1:100.000 in Scale*; Tipografia Valdostana: Aosta, Italy, 2007.
52. Trigila, A.; Iadanza, C.; Spizzichino, D. IFFI Project (Italian Landslide Inventory) and risk assessment. In *First World Landslide Forum*; Springer: Berlin/Heidelberg, Germany, 2008; pp. 18–21.
53. Hughes, P.D.; Gibbard, P.L. A stratigraphical basis for the Last Glacial Maximum (LGM). *Quat. Int.* **2015**, *383*, 174–185. [CrossRef]
54. Wirsig, C.; Zasadni, J.; Christl, C.; Akçar, N.; Ivy-Ochs, S. Dating the onset of LGM ice surface lowering in the High Alps. *Quat. Sci. Rev.* **2016**, *143*, 37–50. [CrossRef]
55. Polino, R.; Malusà, M.G.; Martin, S.; Carraro, F.; Gianotti, F.; Bonetto, F. *Note Illustrative della Carta Geologica d'Italia Alla Scala 1:50.000. Foglio 090 Aosta*; ISPRA-Istituto Superiore per la Protezione e la Ricerca Ambientale: Roma, Italy, 2015; pp. 1–144.
56. Polino, R.; Carraro, F.; Martin, S.; Baggio, P.; Baster, I.; Bertolo, D.; Fontan, D.; Gianotti, F.; Malusà, M.G.; Monopoli, B.; et al. *Carta Geologica d'Italia Alla Scala 1:50.000, Foglio 90, "Aosta"*; ISPRA—Servizio Geologico d'Italia: Roma, Italy, 2015.
57. Elter, G. *Carte Géologique de la Vallée d'Aoste, Echelle 1:100.000. C.N.R.*; Centro Studi sui Problemi dell'Orogeno delle Alpi Occidentali Edizioni S.E.L.C.A.: Firenze, Italy, 1987.
58. De Giusti, F.; Dal Piaz, G.V.; Massironi, M.; Schiavo, A. Carta geotettonica della Valle d'Aosta. *Mem. Sci. Geol.* **2004**, *55*, 129–149.
59. Dal Piaz, G.V.; Bistacchi, A.; Massironi, M. Geological outline of the Alps. *Episodes* **2003**, *26*, 175–180. [CrossRef]
60. Malusà, M. Post-Metamorphic evolution of the Western Alps: Kinematic Constraints from a Multi-Disciplinary Approach (Geological Mapping, Meso-Structural Analysis, Fission-Track Dating, Fluid Inclusion Analysis). Ph.D. Thesis, University of Turin-CNR-IGG, Torino, Italy, 2004; 320p.
61. Forno, M.G.; Gattiglio, M.; Gianotti, F. Geological context of the Becca France historical landslide (Aosta Valley, NW Italy). *Alp. Mediterr. Quat.* **2012**, *25*, 125–139. Available online: https://amq.aiqua.it/index.php/amq/article/view/51 (accessed on 18 October 2021).

62. Forno, M.G.; Gattiglio, M.; Gianotti, F.; Guerreschi, A.; Raiteri, L. Deep-seated gravitational slope deformations as possible suitable locations for prehistoric human settlements: An example from the Italian Western Alps. *Quat. Int.* **2013**, *303*, 180–190. [CrossRef]
63. Forno, M.G.; Gattiglio, M.; Gianotti, F.; Guerreschi, A.; Raiteri, L. La percezione del paesaggio di alta montagna da parte dell'uomo preistorico: L'esempio dell'area di Plan di Modzon nella Conca del Fallère (Valle d'Aosta, Italia nordoccidentale). In Proceedings of the Atti del Convegno in Memoria di Lucilia Gregori, Perugia, Italy, 19–22 February 2013; Cultura Territori e Linguaggi, Università di Perugia: Perugia, Italy, 2014; Volume 4, pp. 233–245.
64. Mercalli, L.; Castellano, C.; Cat Berro, D.; Di Napoli, G.; Guindani, N.; Montuschi, S.; Mortara, G.; Ratti, M. *Atlante Climatico della Valle d'Aosta*; Società Meteorologica Subalpina: Torino, Italy, 2003; 405p.
65. Bajni, G.; Camera, C.A.S.; Apuani, T. Deciphering meteorological influencing factors for Alpine rockfalls: A case study in Aosta Valley. *Landslides* **2021**, *18*, 3279–3298. [CrossRef]
66. Pini, R.; Ravazzi, C.; Raiteri, L.; Guerreschi, A.; Castellano, L.; Comolli, R. From pristine forests to high-altitude pastures: An ecological approach to prehistoric human impact on vegetation and landscapes in the western Italian Alps. *J. Ecol.* **2017**, *105*, 1580–1597. [CrossRef]
67. Brunetti, M.; Maugeri, M.; Nanni, T.; Simolo, C.; Spinoni, J. High resolution temperature climatology for Italy: Interpolation method intercomparison. *Int. J. Climatol.* **2014**, *34*, 1278–1296. [CrossRef]
68. Blanchy, G.; Saneiyan, S.; Boyd, J.; McLachlan, P.V.; Binley, A. ResIPy, an intuitive open source software for complex geoelectrical inversion/modelling. *Comput. Geosci.* **2020**, *137*, 104423. [CrossRef]
69. Binley, A. Tools and techniques: DC Electrical Methods. In *Treatise on Geophysics*, 2nd ed.; Elsevier: Amsterdam, The Netherlands, 2015; Volume 11, pp. 233–259. [CrossRef]
70. Gouffon, Y. Géologie de la "nappe" du Grand St-Bernard entre la DoireBaltée et la frontière suisse (Vallée d'Aoste, Italie). *Mém. Géol.* **1993**, *12*, 150.
71. Pantet, A.; Epard, J.L.; Masson, H. Mimicking Alpine thrusts by passive deformation of synsedimentary normal faults: A record of the Jurassic extension of the European margin (Mont Fort nappe, Pennine Alps). *Swiss J. Geosci.* **2020**, *113*, 13. [CrossRef]
72. Caby, R. Le Mesozoique de la zone du Combin en Val d'Aoste (Alpes Graies): Imbrications ectoniques entre series issues des domaines pennique, austroalpin et oceanique. *Géol. Alp.* **1981**, *57*, 5–13.
73. Dal Piaz, G.V. Alcune considerazioni sulla genesi delle ofioliti piemontesi e dei giacimenti ad esse associati. *Bolettino Assoc. Mineraria Subalp.* **1971**, *8*, 365–388.
74. Bearth, P. Zur Gliederung der Bundnerschiefer in der Region von Zermatt. *Eclogae Geol. Helv.* **1976**, *69*, 149–161.
75. Chessex, R. Tectonomagmatic setting of the Mont Fort nappe basement, Penninic Domain, Western Alps, Switzerland. In *International Earth Sciences Colloquium on the Aegean Region*; Piskin, O., Ergun, M., Savascin, M.Y., Tarcan, G., Eds.; Izmir: Gulluck, Turkey, 1995; Volume 1, pp. 19–35.
76. Sartori, M.; Gouffon, Y.; Marthaler, M. Harmonisation et définition des unités lithostratigraphiques brianconnaises dans les nappes penniques du Valais. *Eclogae Geol. Helv.* **2006**, *99*, 363–407. [CrossRef]